THESIS

SUBSURFACE MAPPING OF THE ROSS ISLAND FLEXURAL BASIN, SOUTHWEST ANTARCTICA

Submitted by

Christopher P. Wenman

Department of Geosciences

In partial fulfillment of the requirements

For the Degree of Master of Science

Colorado State University

Fort Collins, Colorado

Summer 2016

Master's Committee:

Advisor: Dennis Harry

Sven Egenhoff
Michael Gooseff

ABSTRACT

SUBSURFACE MAPPING OF THE ROSS ISLAND FLEXURAL BASIN,
SOUTHWEST ANTARCTICA

Ross Island is a post-Miocene (< 4.6 Ma) volcanic island located in the Ross Sea region of southwest Antarctica. This region of Antarctica borders the western edge of the West Antarctic Rift System, along the Transantarctic Mountain front. Marine and over-ice multi-channel seismic reflection surveys and borehole studies targeting the Ross Sea region over the last 30+ years have been used in this study to develop a seismic stratigraphic model of the development and evolution of the Ross Island flexural basin. Four key stratigraphic horizons were identified and mapped to fully capture the basin-fill, as well as strata lying above and below the flexural basin. From oldest to youngest these horizons are named RIB-m, RIM-g, RIM-b and RIB-r. Time structure, isochron and isochore maps were created for the horizons and the stratigraphic intervals they bound. The seismic stratigraphic record shows the Ross Island flexural moat formation post-dates the main tectonic subsidence phase within the Victoria Land Basin. The maps presented here are the first to fully illustrate the evolution of the Ross Island flexural basin. The maps highlight depositional patterns of two distinct periods of flexural subsidence and basin-filling superimposed on the older N-S trending Victoria Land Basin depocenter. Two units of flexural basin fill, Unit FFI between horizons RIM-g and RIM-b (the oldest flexural basin fill), and Unit FFII between horizons RIM-b and RIB-r (the youngest flexural basin fill) are associated with the two periods of flexural subsidence. Flexural moat subsidence and subsequent filling occurred episodically during periods of active volcanism on

the island. Unit FFI is estimated to range from ca. 4 to 2 Ma, corresponding with formation of the Mt. Bird volcanic edifice on Ross Island. Unit FFII ranges in age from ca. 2 to 1 Ma, and is related to Mt. Terror, Mt. Erebus, and Hut Point Peninsula volcanism. The isochore maps suggest the depocenter of the flexural basin during both time intervals was located north of the island, instead of directly beneath the Ross Island topographic load. Factors contributing to the northerly location of the depocenter include i) volcanic loading by McMurdo Volcanic Group subsea volcanic features north of the island, ii) partial compensation of the main Ross Island load by low-density, partially molten rock beneath the island, iii) extensional faulting within the Terror Rift, and iv) seaward-thickening shelf sediments transported from the Ross Ice Shelf. The seismic data show that the onset of filling of the flexural moat around Ross Island coincided with the end of ice grounding events in the area. We infer that this was caused by flexural subsidence of the seafloor to accommodate the Ross Island load.

ACKNOWLEDGEMENTS

Many thanks to the following scientists for their contributions to this project - Christopher Sorlien (UC Santa Barbara; original data set and TKS project), Huw Horgan (Victoria University of Wellington; HPP and MIS seismic surveys) and Marvin Speece/Steve Pekar (Montana Tech/Queens College; ONH, ATS and MSV seismic surveys).

I would also like to thank my advisor, Dennis Harry, and committee members, Sven Egenhoff and Mike Gooseff, for their support and guidance throughout this project.

Thank you to Sumant Jha for participating in many helpful discussions as I progressed through this work.

And a final thank you to my family, fellow graduate students, friends, and especially my fiancé AnnMarie, for their support and for making my time at CSU memorable.

TABLE OF CONTENTS

CHAPTER 1 – INTRODUCTION

The Antarctic continent, covered in ice since the Oligocene Epoch, plays a key role in recording and providing a study area to understanding the drivers affecting the global climate record. The study of the Antarctic ice sheet response to global climate change in the geologic past becomes increasingly important to inform studies of how modern ice sheets on the continent (the West Antarctic Ice Sheet, Ross Ice Shelf, and East Antarctic Ice Sheet) will respond to modern climate forcing related to the increase of CO_2 emissions. The climate record contained in the Antarctic stratigraphy is found to be closely related to, and moderated by, tectonic activity. Of particular importance is the West Antarctic Rift System, a region of active tectonism and volcanism since the Late Cretaceous that separates the East Antarctic Craton from Marie Byrd Land and West Antarctica (Lawver and Gahagan, 1994; Weaver et al., 1994; Luyendyk, 1996, 2001, 2003; Cande, 2000; Mukasa and Dalzial, 2000. This region encompasses the particularly vulnerable West Antarctic Ice Sheet (WAIS), as well as the Ross Ice Shelf. The WAIS has been identified as a key piece of the climate change puzzle, as it is capable of catastrophic collapse both in the past and future (Pollard and DeConto, 2009). The Ross Sea region has been the target of considerable research since the 1980s to identify and recover pieces of the stratigraphic record lying below the Ross Sea and Ross Ice Shelf that are not available on the Antarctic continent itself. This research has included geophysical surveys (e.g. marine multi-channel seismic, over-ice seismic, aeromagnetics, aerogravity) and complementary borehole drilling projects in order to identify the lithostratigraphy and map the units throughout the Ross Sea.

This thesis focuses on the post-Miocene tectonic evolution of the area around Ross Island in the southern Ross Sea near the terminus of the modern WAIS and Ross Ice Shelf. The time

period from the Pliocene to recent has been characterized by dynamic waxing and waning of the ice sheet that was potentially influenced by both climatic and tectonic controls (Naish et al., 2007b). This thesis focuses on the formation of an enclosing flexural basin (or flexural moat) around Ross Island as it was built over the past 4.6 Ma and develops an integrated stratigraphic model of the spatial and temporal evolution of the Ross Island flexural basin based on the seismic stratigraphy and borehole data in the region. The key findings from the study are: 1) Ross Island volcanic loading depressed the flexural moat below the ice grounding line ca. 4 Ma, effectively de-coupling the tectonic and climatic signals in the stratigraphic record within the moat; 2) the Ross Island flexural moat, and related younger volcanics to the north, developed after the main tectonic phase of Victoria Land Basin (VLB) subsidence, but were coeval with strata deposited during the phase of slow thermal subsidence of the VLB; 3) filling of the flexural moat around Ross Island occurred in two distinct phases following periods of rapid subsidence induced by volcanic loading; and 4) the primary post-VLB depocenter resulting from flexural subsidence due to volcanic loading is located north of Ross Island, implying substantial subsurface density variation in the Ross Island region, or recent tectonism and/or volcanism north of the island. The IHS Kingdom Suite project containing all of the data, interpretations, and maps is archived on the servers in the CSU Department of Geoscience.

CHAPTER 2 – SUBSIDENCE AND FILLING OF THE ROSS ISLAND FLEXURAL MOAT, ROSS SEA, SOUTHWEST ANTARCTICA

2.1 INTRODUCTION

Ross Island is a post-Miocene (<4.6 Ma) volcanic island located in the Ross Sea region of southwest Antarctica along the Transantarctic Mountain Front within the western part of the West Antarctic Rift System (Figure 1). Seismic surveys completed across the Ross Sea over the last 30+ years suggest that the island is at least partially surrounded by a moat-like flexural basin. Drilling results show that the flexural basin contains up to 1.2 km of sedimentary strata (Naish et al., 2007b). Cores recovered from drilling in the flexural basin indicate the basin-fill strata consist of late Miocene and younger volcaniclastic, glaciomarine and marine sediments (Krissek et al., 2007; Naish et al., 2007b; Wilson et al., 2007).

As distinct volcanic eruptions constructed Ross Island, rapid flexural subsidence occurred in response to the volcanic load, creating accommodation space for sediment infilling. This subsidence and subsequent sedimentation into the flexural basin results in a nearly complete, high-resolution stratigraphic record of basin history from inception to filling. This record allows us to distinguish individual periods of flexural subsidence and the resulting basin filling events that are hypothesized to be associated with crustal loading during distinct volcanic episodes on Ross Island.

Horgan et al. (2005) used seismic stratigraphic relationships in a preliminary study of the flexural moat on the south side of Ross Island to identify three episodes of flexural subsidence that were tentatively related to volcanic events on Ross Island. Additional work on the flexural seismic stratigraphy was compiled in Naish et al. (2007a), where workers correlated the flexural

stratigraphy from the south side of Ross Island to seismic lines on the west side of Ross Island. Fielding et al. (2008) merged the stratigraphic interpretation within the Ross flexural moat with their regional seismic stratigraphic synthesis. While the seismic stratigraphy of the flexural moat has been identified and partially mapped by these previous workers, no attempt has been made to correlate in detail the seismic stratigraphy of the flexural moat in the context of the basin evolution as a whole.

In this paper, we use 2D seismic reflection data correlated to the ANDRILL and CIROS boreholes that are located near the island to develop a complete model for basin subsidence and filling since about 4.6 Ma. We identify at least 2 episodes of flexural down-warping, followed by sediment filling of the resulting basin, which we correlate with individual volcanic loading events associated with the construction of Ross Island.

2.2 GEOLOGIC BACKGROUND

Tectonics of the West Antarctic Rift System

Ross Island is located near the western flank of the West Antarctic Rift System (WARS) in the southwestern Ross Sea (Figure 1). The WARS is a broad, late Cretaceous through at least Pleistocene age rift system that is characterized by two distinct phases. The first phase initiated ca. 110 Ma and ended ca. 83 Ma. This phase of rifting formed a 750 to 1000 km wide extensional province in the Ross Sea embayment between the East Antarctic Craton (EAC) to the west and Marie Byrd Land (MBL) to the east (Lawver and Gahagan, 1994; Weaver et al., 1994; Luyendyk, 1996, 2001, 2003; Cande, 2000; Mukasa and Dalzial, 2000). The area is estimated to have stretched by 25 to 50% to accommodate several hundred kilometers of extension between the EAC and MBL (Behrendt et al., 1991; Cande et al., 2000; Huerta and Harry, 2007; Aitken et al., 2012). Four major north-south trending, fault-bounded sediment-filled basins separated by

two shallow basin platforms were formed during Late Cretaceous rifting. From east to west these are the Eastern Basin, Central High, Central Basin, Coulman High, Victoria Land Basin and Northern Basin (Figure 1). These features were originally identified in marine multi-channel seismic (MCS) surveys carried out in the 1980s and 1990s (Hinz and Block, 1984; Cooper et al., 1987, 1991). The sedimentary strata filling the basins was drilled and dated from the Late Oligocene to recent by multiple drilling projects (See "Regional Seismic Stratigraphy and Borehole Studies" section below). The sedimentary basins are associated with positive Free Air gravity anomalies (Behrendt et al., 1991; Karner et al., 2005). The presence of the positive Free Air gravity anomalies has been explained by a shallow dense mantle or deep crustal intrusions lying below the basins (Hayes and Davey, 1975; Davey and Cooper, 1987; Behrendt et al., 1991, Cooper et al., 1991). Preservation of these gravity anomalies is due to an increase in the flexural rigidity of the lithosphere between basin formation and basin filling, suggesting the basins are pre-Cenozoic (Karner et al., 2005).

The Late Cretaceous style of broadly distributed rifting and basin subsidence continued into the Paleogene Period. This was accompanied by uplift of the Transantarctic Mountains beginning ca. 55 Ma (Fitzgerald, 1992) and the deposition of large thicknesses of Oligocene sediments within the four major rift basins and covering the inter-basin platforms (Cande et al., 2000). The Oligocene was also marked by the appearance of the Marie Byrd Land dome, hypothesized to be the result of a mantle plume (Hole and LeMasurier, 1994; LeMasurier and Landis, 1996). Seafloor spreading in the Adare Trough, located north of the Northern Basin, occurred between 46 and 25 Ma - soon after uplift of the Transantarctic Mountains and contemporaneously with extension in the Ross Sea (Cande et al., 2000; Davey et al., 2006; Decesari et al., 2007; Muller et al., 2007). Magnetic anomalies in the Adare Basin can be traced

into the Northern Basin, suggesting a tectonic relationship between the two basins (Muller et al., 2005; Cande and Stock, 2006).

The second phase of rifting in the WARS consisted of Neogene tectonic and volcanic activity focused primarily on the western flank of the rift along the Transantarctic Mountain (TAM) front, in Northern Victoria Land, and within the Victoria Land Basin and the Northern Basin (Davey et al., 2000). Uplift of the TAMS ended during the early part of the second phase of rifting, by ca. 17 Ma (Davey et al., 2001). Due to the focused phase of rifting along the western flank, the WARS became an asymmetrical rift system marked on the western flank by a 3000-km long, 4- to 5-km high rift shoulder escarpment along the TAM from northern Victoria Land to the Ellsworth Mountains (Behrendt, 1999) and on the east by the Marie Byrd Land dome.

Neogene extension in the WARS focused primarily along the western flank of the rift and in the Victoria Land Basin (VLB), the deepest sedimentary basin in the Ross Sea region. The VLB is a 150-km wide extensional half-graben filled with up to 14 km of sedimentary rocks based on MCS data and gravity model studies (Hinz and Block, 1984; Davey and Cooper, 1987; Cooper et al., 1987, 1991). The lower 8 km of the basin fill consists of high p-wave velocity (4.2-6.0 km/s), faulted, Mesozoic strata lying below a distinct Late Oligocene unconformity (Cooper et al., 1987; 1991). Above the unconformity, 6 km of flat-lying, faulted, lower p-wave velocity (1.7-4.1 km/s) Cenozoic strata complete the basin fill (Cooper et al., 1987; 1991). The VLB strata are very similar to the strata identified by MCS studies conducted in the Eastern Basin and Central Basin (i.e. Hinz and Block, 1984; Cooper et al., 1987, 1991), where up to 6 km of sedimentary rock with p-wave velocities of 1.9 to 3.8 km/s unconformably overlay thick, high-velocity strata (Hinz and Block, 1984; Cooper et al., 1991). However, in the Eastern and

Central Basins, the strata above the Oligocene unconformity are relatively un-faulted (Hinz and Block, 1984).

In the central part of the VLB is the younger, Cenozoic-age Terror Rift. The Terror Rift extends along strike within the central VLB from the active volcanoes at Cape Washington, south to Ross Island (Davey and Cooper, 1987) (Figure 1). The Terror Rift consists of the Discovery Graben, a 25-35 km-wide faulted axial graben, and a 25-40 km-wide fault-bounded horst, cutting basement and syn-tectonically erupted subaerial volcanics (Cooper et al., 1987, 1991). Strata within the Terror Rift are offset by Pleistocene age faults in the shallow subsurface, sometimes cutting the seafloor, showing continuing deformation in this region at least into the Pleistocene. In places, the Terror Rift strata are interrupted by intrusive magmatic rocks of the Cenozoic McMurdo Volcanic Group (Cooper et al., 1987; Fielding et al., 2006, 2008; Henrys et al., 2007).

Regional Seismic Stratigraphy and Borehole Studies

Various core drilling projects and seismic reflection surveys have been completed throughout the Ross Sea, with recent emphasis in the McMurdo Sound region near Ross Island. The earliest drilling aimed at core recovery in the Ross Sea was completed during Leg 28 of the Deep Sea Drilling Project (DSDP), where four boreholes were drilled – DSDP 270, 271, 272 and 273. Sites 270, 271 and 272 were drilled in 1973 on the edge of the Eastern Basin (Figure 1), where nearly 1100 m of core was recovered from a glaciomarine stratigraphic sequence dated from the Oligocene to recent (Hayes and Frakes, 1975). Site 273 was drilled in 1973 on the flank of the Central Trough north of Ross Island (Figure 1), where recovery of a ~346 m-long glaciomarine stratigraphic sequence was dated to the Mid-Miocene, with a condensed or missing post-Miocene portion of the section removed by glacial erosion ca. 3-5 Ma (Hayes and The

Shipboard Scientific Party, 1975b). A key finding of DSDP Leg 28 Site 270 was the identification of a Late Oligocene unconformity (ca. 25 Ma), interpreted to represent the onset of Antarctic glaciation (Hayes and Frakes, 1975). Additionally, the DSDP Leg 28 sites encountered a distinct erosional unconformity covering a hiatus from the Early Pliocene to Late Miocene when grounded ice advanced northward sometime ca. 5.0 Ma compared to the current position of the Ross Ice Shelf (Hayes and Frakes, 1975; Hayes and The Shipboard Scientific Party, 1975a).

Following the DSDP project, the 1979 McMurdo Sound Sediment and Tectonic Studies (MSSTS) project drilled the MSSTS-1 borehole west of Ross Island in the McMurdo Sound region to a depth of 230 meters below sea floor (mbsf) and recovered a Late Oligocene (ca. 29 Ma) through recent glaciomarine stratigraphic sequence (Barrett et al., 1987) (Figure 2). Later drilling and magnetostratigraphy work in the McMurdo Sound region at the CIROS-1 site revised the bottom hole age date in MSSTS-1 to ca. 27 Ma (Harwood et al., 1989). The rocks encountered in the MSSTS-1 borehole were deposited in a shallow, near shore marine environment with strong glacial influence, suggesting glaciers have persisted in the region since the Late Oligocene (Barrett and McKelvey, 1981).

The first major seismic reflection study was completed by Hinz and Block (1984) in the central and northern Ross Sea, who identified and traced regional unconformities (named U1 to U6 from youngest to oldest) in the Oligocene and younger sediments in the Eastern Basin and Central Trough. The unconformities bound what they interpreted as marine delta lobes (with the corresponding seismic sequences named RS-1 through RS-5 from youngest to oldest). Most notable was U6, which was traced to the Late Oligocene unconformity, drilled at DSDP Site 270 where basal glacial sediments are 25 Ma above U6, and pre-glacial greensands below were dated to 26 Ma. U6 and older units were found to pinch out against the Central High, making

correlation of older units into the western Ross Sea difficult. Davey and Christoffel (1984) correlated seismic reflection data in the western Ross Sea to the MSSTS-1 borehole, providing the first offshore age control for the stratigraphy in the central and western Victoria Land Basin. They determined the sedimentary sequence lying below McMurdo Sound between Ross Island and the MSSTS-1 drill site to the west is mainly early Tertiary or older in age, with a post-Eocene section that is <800 m thick. This study also identified a major erosional unconformity from Late Eocene to Late Oligocene, named "hiatus Y" (after Webb, 1983), coinciding with the Late Oligocene unconformity encountered in DSDP Site 270 (Hayes and Frakes, 1975b) and identified in seismic data and traced into DSDP Site 270 by Hinz and Block (1984).

To further constrain sediment ages and interrogate the glacial history of the McMurdo Sound region, the 1986 Cenozoic Investigations in the Western Ross Sea (CIROS) project drilled the CIROS-1 borehole 702 mbsf into a glaciomarine sequence just south of the MSSTS-1 borehole (230 mbsf), providing nearly 500 m of additional geologic data for the rocks underlying McMurdo Sound (Barrett et al., 1991) (Figure 2). The recovered core contains marine sedimentary rocks from the Lower Miocene to the Latest Eocene/Earliest Oligocene in age (ca. 36 to 22 Ma) (Harwood et al., 1989; Wilson et al., 1998). An erosional unconformity representing the onset of glaciation ca. 28.5 to 28 Ma was identified at 366 mbsf, and accounted for nearly 4 m.y. of missing Oligocene strata (Harwood et al., 1989; Wilson et al., 1998). The Late Oligocene unconformity identified in this borehole was correlated with the major unconformity U6 in the Central and Eastern Basins of Hinz and Block (1984) and hiatus Y in McMurdo Sound of Davey and Christoffel (1984), indicating the unconformity represents a Ross Sea-wide continental glaciation (Bartek et al., 1991). The Ross Sea-wide expanse of the

Late Oligocene unconformity has been confirmed in later seismic studies (e.g. Anderson and Bartek, 1992; Barrett et al., 1995).

Cooper et al. (1987) presented the first comprehensive regional seismic stratigraphic framework for the western Ross Sea and Victoria Land Basin. Their framework divided the stratigraphy into 7 seismic units, termed V1 through V7, building on the earlier seismic stratigraphic studies by Hinz and Block (1984) and Davey and Christoffel (1984) in the central and northern Ross Sea (Table 1). Their work agreed with the seismic tie to the MSSTS-1 borehole presented by Davey and Christoffel (1984) using "hiatus Y", the distinct Late Oligocene unconformity. They also tied the Late Oligocene unconformity imaged in the CIROS-1 core and in seismic reflection data from the eastern side of the VLB to the unconformities mapped by Hinz and Block (1984) in the central and northern Ross Sea, but noted that the tie was uncertain due to pinch-outs on the Central High (just as in Hinz and Block, 1984).

Anderson and Bartek (1992) reported results of the 1990 Polar Duke (PD90) cruise, which collected single channel seismic reflection data across the entire Ross Sea, from the Eastern Basin west to the Victoria Land Basin. The goal of the study was to provide a high resolution record of the Oligocene and younger strata with sufficient coverage to tie the DSDP, MSSTS-1 and CIROS-1 boreholes together using the new seismic data set. They identified 13 seismic units in the Eastern Basin (Unit 1 to Unit 13) (Table 1), the oldest of which (Unit 13) underlies the distinct Late Oligocene unconformity. Direct ties of the late Oligocene to early Miocene strata in the Victoria Land Basin to the time-equivalent units of the Eastern Basin was hindered by pinch-outs against the Central High (similar to the problem encountered in Hinz and Block, 1984 and Cooper et al., 1987) and due to heavy erosion of Miocene strata in the western Ross Sea (Anderson and Bartek, 1992). The study also concluded that the Plio-Pleistocene

section was limited in distribution on the western shelf when compared to the eastern Ross Sea (Anderson and Bartek, 1992).

Brancolini et al. (1995) generated a general seismic facies model for the western Ross Sea, including the Victoria Land Basin and the Northern Basin, identifying seismic sequences RSS1-8 bound by unconformities RSU1-6 (Table 1). The oldest sequence in the study, RSS1 (bound on the top by RSU6), was well developed in the Northern Basin, and was hypothesized to be sampled in the CIROS-1 borehole in the Victoria Land Basin. RSU6 could coincide with the Late Oligocene unconformity sampled at 366 mbsf in CIROS-1, but the tie was tentative due to interference from post-Oligocene faulting moving out of the VLB to the CIROS-1 drill site (Brancolini et al., 1995). They also determined that there was massive erosion by polar ice sheets at the shelf edge since at least early Pliocene time and postulated that eustasy was the main control on depositional environments in the Ross Sea, including grounded ice deposits.

Barrett et al. (1995) and Bartek et al. (1996) identified 20 seismic sequences, labeled A-T (Table 1), in single channel data in the western Ross Sea that were correlated to the MSSTS-1 and CIROS-1 boreholes to present a detailed seismic stratigraphic subdivision of the Cenozoic section in the McMurdo Sound, and as preliminary work for the Cape Roberts Project (CRP) boreholes. The CRP boreholes, CRP-1, -2 and -3, were drilled from 1997 to 1999 in the western Ross Sea, north of the CIROS-1 and MSSTS-1 boreholes (Figure 2). The total section recovered provided nearly 1500 m of core that provided a discontinuous record of Late Eocene to Early Miocene sedimentation and paleoclimate variation (Florindo et al., 2005). The rocks encountered in CRP-3 and CRP-2 were dated from ca. 34 Ma to ca. 17 Ma, with a minor section in CRP-1 dated from 5 Ma to recent. The identification of glaciomarine sediments that dated to ca. 34 Ma in CRP-3 confirmed the presence of a cold climate in the VLB since earliest Oligocene times

(Cape Roberts Science Team, 2000). Another noteworthy discovery was made at 823 mbsf in the CRP-3 borehole, where the oldest Cenozoic strata (ca. 34 Ma) were unconformably overlying Devonian Beacon Supergroup sandstones, representing a 300 m.y. hiatus (Cape Roberts Science Team, 2000). The Cape Roberts Project also revised the "V" nomenclature of Cooper et al. (1987), making most reflectors much younger than originally thought. Namely the V3/V4 seismic boundaries (Cooper et al., 1987) represent 21 Ma (Early Miocene) and 27 Ma (Late Oligocene) surfaces. Fielding et al. (1998, 2000, 2001) performed sequence stratigraphic and facies architecture studies on the CRP-1, -2, and -3 boreholes, respectively, in order to establish a tectono-stratigraphic model for the CRP succession. The tectono-stratigraphic model was based on work by Henrys et al. (2000, 2001) who used vertical seismic profiles from the CRP-2 and -3 holes to precisely correlate reflection events to changes in the lithology found in the core. The Cape Roberts Project strata also helped to determine a subsidence history for the Victoria Land Basin based on sediment accumulation rates (Florindo et al., 2005) and basin subsidence studies (De Santis et al., 2001). They inferred rapid subsidence occurred from 34 to 31 Ma, with subsidence slowing until 17 Ma, and no net subsidence after 17 Ma.

Horgan et al. (2005) completed a seismic stratigraphic analysis near Hut Point Peninsula southeast of Ross Island to provide a site assessment for the Antarctic Geologic Drilling (ANDRILL) McMurdo Ice Shelf (MIS) AND-1B borehole. They identified three distinct seismic stratigraphic facies, Unit I-III, bound by five distinct reflectors (Table 1). The three facies were identified as distinct episodes of flexural moat fill on the southeastern side of Ross Island, which they correlated to accommodation space created during discrete phases of subsidence due to individual volcanic loading events. Unit III consists of normal faulted, generally low-amplitude seismic reflectors that were accumulated after emplacement of Mount Bird. Unit II contains

generally high amplitude, continuous reflectors that onlap Unit III and were deposited in accommodation space created by Mount Terror crustal loading. Unit IB is described as seismically opaque to low-amplitude reflectors that onlap Unit II from Mount Erebus loading c. 1.0 Ma. Unit IA consists of high-amplitude reflectors from strata deposited during Mount Erebus loading c. 0.8 Ma.

The most recent drilling project was the Antarctic Geologic Drilling (ANDRILL) program that drilled two boreholes near Ross Island. In 2006 the McMurdo Ice Shelf (MIS) borehole, known as AND-1B, was drilled 10 km east of Hut Point Peninsula on the southeast side of Ross Island (Figure 2). The drilling target was strata filling the flexural moat surrounding Ross Island (Naish et al., 2007a). Lithologies recovered from the borehole include siliciclastic and volcanic diamictites, sandstones and mudstones, diatomites, volcanic ashes and tuffs, and one lava flow (Krissek et al., 2007; Naish et al., 2007b). These strata provided a high-resolution, thick Plio-Pleistocene succession that was previously only recovered in condensed section within the CRP-1 core. The ANDRILL Southern McMurdo Sound (SMS) borehole, known as AND-2A, was drilled in 2007 west of Ross Island on a stratigraphic high, south of the CIROS-1 and MSSTS-1 boreholes where the strata provide additional chronostratigraphic control for seismic surfaces identified in the extensive grid of seismic lines that cover the McMurdo Sound region (Florindo et al., 2008) (Figure 2). Sediments in the core have been described generally as amalgamated, ice-proximal diamictites with a sandstone dominated interval associated with a regional Early Pliocene relative sea-level high stand ca. 5-4 Ma (Fielding et al., 2011). The recovered strata support the presence of repeated fluctuations in climate, ice expansion and contraction, and sea-level change from the Early- to Mid-Miocene (c. 20.2 to 14.2 Ma), with a

thin, discontinuous record of sediments <14 Ma overlying a major unconformity at 224.82 mbsf (Fielding et al., 2011).

Fielding et al. (2006) presented a new seismic stratigraphic framework for the entire McMurdo Sound region, using core to seismic ties at the Cape Roberts Project boreholes and expanding outwards to the available seismic and borehole data at the time. They divided the Victoria Land Basin fill into five tectono-stratigraphic phases (similar results to what Cooper et al., 1987 did) – Regional Uplift and Erosion (Early Cenozoic, pre-34 Ma), Early Rift (Latest Eocene to Early Oligocene, 34-29 Ma), Main Rift (Oligocene, 29-24 Ma), Thermal Subsidence (Early Miocene, 24-<17 Ma), and Terror Rift formation (<17 Ma). Naish et al. (2007b) correlated the reflectors identified in the flexural moat by Horgan et al. (2005) and elsewhere by Fielding et al. (2006) to the AND-1B borehole and completed time-depth conversions to provide lithostratigraphic control on the southeast side of the island.

Fielding et al. (2008) revised the Fielding et al. (2006) findings by further interpreting the youngest portion of the stratigraphy based on previous work by Horgan et al. (2005) and Naish et al. (2007b), expanding the flexural horizon interpretation to the west side of Ross Island. The five rift phases were slightly revised to – Exhumation of the Transantarctic Mountains, Early Rift, Main Rift, Passive Thermal Subsidence, a lower interval of Renewed Rifting and an upper interval of Renewed Rifting. This study associated the onset of flexural loading with a distinctive reflector in the seismic data, named the Rj reflector (Table 1). Pekar et al. (2013) completed the most recently published seismic interpretation in the McMurdo Sound region using the reflectors from Fielding et al. (2008) to correlate across the Offshore New Harbor (ONH) (Sunwall et al., 2012) and Arctic Thunder Sled (ATS) (Betterly et al., 2007; Speece et al., 2009) MCS surveys to provide a tie between the AND-2A and CIROS-1 boreholes.

Volcanics of the West Antarctic Rift System

Volcanism in the WARS region began on the eastern flank of the rift (MBL and the Antarctic Peninsula) with subduction-related calc-alkaline magmatism that dates back at least to the early Carboniferous (Mukasa & Dalziel, 2000). During this period, West Antarctica, New Zealand, and the Campbell Plateau were located on the over-riding plate of the Gondwana convergent margin (Storey et al., 1992; Davey and Brancolini, 1995; Weaver, 1994; Luyendyk, 1995; Eagles, 2003; Eagles et al., 2004, 2009; Torsvik et al., 2007). The oldest intrusive subduction related calc-alkaline rocks in MBL are I-type granites dated from ca. 320 ± 3 Ma to 110 ± 1 Ma (Weaver et al., 1994). Subduction ceased ca. 110 Ma (Mukasa and Dalzial, 2000; Weaver et al., 1994), when the Pacific-Phoenix ridge collided with the convergent margin. At this time, the West Antarctic back-arc plateau collapsed and rifting and rift-related magmatism began rapidly. Age dating of rift-related magmatic rocks – A-type syenite intrusions (ca. 100 ± 2 Ma) and A-type metaluminous to peralkaline granites (ca. 102 to 95 Ma) – suggest rift-related alkaline magmatism in MBL began less than 10 Myr after subduction ceased (Mukasa and Dalzial, 2000; Weaver et al., 1994).

Alkaline magmatism was renewed on the eastern flank of the WARS in MBL in the Oligocene (ca. 30-25 Ma) and continued until as recently as ca. 0.82 Ma (Kyle, 1990; LeMasurier and Rex, 1991; Hole and LeMasurier, 1994; LeMasurier and Landis, 1996; Mukasa and Dalziel, 2000; Rilling et al., 2007). It has been proposed that a mantle plume fed initial Cenozoic magmatism in MBL, as the trace element and isotopic composition of MBL basalts is similar to Ocean Island Basalts (OIB) that result from plume activity (Hole and LeMasurier, 1994; LeMasurier and Landis, 1996). The Cenozoic plume model is supported by syn-volcanic (ca. 30-28 Ma) doming of MBL, rising nearly 2700 m above sea level (Hole and LeMasurier,

1994; LeMasurier and Landis, 1996). Isotopic and large-ion lithophile element (LILE) data suggest that the Cenozoic plume that fed Marie Byrd Land may have fed magmatism across the WARS, where OIB-like rock compositions are common (Hole and LeMasurier, 1994, LeMasurier and Landis, 1996; Weaver et al., 1994; Sieminski et al., 2003; Esser et al., 2004). A change has been identified in rocks from MBL that are younger than ca. 12 Ma, when basalt compositions change from OIB-like to resemble Mid-Ocean Ridge Basalts (MORB) as Mg-number and Sr isotopic ratios decreased (Hole and LeMasurier, 1994).

Alkaline magmatism in the western Ross Sea along the Transantarctic Mountain front has been dated to the Late Eocene and younger (ca. 48 Ma to recent) (LeMasurier and Rex, 1991; Kyle, 1990; Hole and LeMasurier, 1994; Mukasa and Dalziel, 2000, Rilling et al., 2007). Along the Transantarctic Mountain front, syn-rift magmatism is dominated by under-saturated alkaline (OIB-like) rocks, specifically alkali-rich olivine basalts, trachytes and phonolites (Kyle and Cole, 1974). The north-south oriented belt of alkaline volcanic provinces in the western portion of the Ross Sea along the mountain front is named the McMurdo Volcanic Group (Kyle and Cole, 1974; Kyle 1990).The McMurdo Volcanic Group consists of three separate provinces that are defined on the basis of spatial distribution and tectonic setting (Kyle and Cole, 1974; Kyle, 1990). These include i) the Hallett Province (13 Ma to <10 Ma); ii) the Melbourne Province (25 Ma to <0.5 Ma); and iii), the most recently active Erebus Province (19.8 Ma to present) (Kyle, 1990). The Erebus Volcanic Province is located at the southern end of the Terror Rift in an area marked by a change in the strike of the TAM, where several fault zones bounding the TAM intersect (Kyle 1990). The syn-rift magmatism in the Erebus province consisted of intermittent eruptions from scattered volcanic centers during an episode of continental glaciation dating back to at least 4.6 Ma (Armstrong, 1978).

A distinct magmatic hiatus, or perhaps a lack of rocks available for sampling, exists between the Mesozoic calc-alkaline rocks and Cenozoic alkaline rocks of the WARS. Strong aeromagnetic anomalies identified across the Ross Sea and West Antarctic Ice Sheet have been interpreted as volcanic rocks of an unknown age (Behrendt et al., 1994, 1996). Based on the aeromagnetic data, it is estimated that the volume of unsampled magmatic rocks in the Ross Embayment exceeds 10^6 km^3 (Behrendt, 1999). It has been postulated that the rocks may be associated with the initial Mesozoic rifting or the later Cenozoic volcanics that extend from Marie Byrd Land west to the TAM front (Behrendt et al., 1991, 1994, 1996; Behrendt, 1999), potentially sourced from a WARS-wide mantle plume (Hole and LeMasurier, 1994; LeMasurier and Landis, 1996; Sieminski et al., 2003; Esser et al., 2004).

Geology and Geodynamics of Ross Island

Ross Island has formed over roughly the past 4.6 Ma as part of the Erebus Volcanic Province, a subset of the McMurdo Volcanic Group that includes (further south) Mount Discovery, Mount Morning, Minna Bluff and many smaller volcanic centers (e.g. White and Black Islands, Brown Peninsula) (Kyle and Cole, 1974; Armstrong, 1978; Kyle 1990). Ross Island was built by distinct episodes of volcanism from four volcanic centers – Mount Bird (4.6 to 3 Ma), Mount Terror (1.8 to 0.8 Ma), Hut Point peninsula (1.3 Ma to 0.4 Ma), and Mount Erebus (1.3 Ma to recent) (Armstrong, 1978; Esser et al., 2004 via K-Ar and $^{40}Ar/^{39}Ar$ dating, respectively) (Fig. 2). As volcanic eruptions formed the island and loaded the crust, the surrounding lithosphere responded to the load by down-warping, resulting in formation of a sub-circular flexural moat. This flexural basin then provided accommodation space for sediments to in-fill. The sediment filling the flexural basin was drilled and cored by the AND-1B borehole (total depth = 1285 m, maximum age = 13.57 ± 0.13 Ma) (Naish et al., 2007b; Wilson et al.,

2007). Lithologies encountered include siliciclastic and volcanic diamictites, sandstones and mudstones, diatomites, volcanic sandstones, volcanic ash and tuff, and one lava flow (Krissek et al., 2007; Naish et al., 2007b). The lithologies and age dates from the AND-1B core have been used as indicators of the climate during deposition, with diamictites deposited under cold polar conditions marked by constant ice sheets (dominant ca. 1-0 Ma) and pelagic diatomites reflecting a slightly warmer climate marked by subpolar ice sheets and interglacial periods (dominant ca. 5-2 Ma) (Naish et al., 2007b; Wilson et al., 2007).

The first geodynamic modeling of flexure around the Ross Archipelago was done by Stern et al. (1991), who produced a model for the flexure of the lithosphere under loading by the entire Ross Archipelago, taken to include Ross Island, White Island, Black Island, Mount Discovery and Mount Morning. They used a semi-infinite (broken) elastic plate model that resulted in a maximum lithosphere deflection of roughly 1800 m with a 100 m high flexural bulge at a distance of 200 km from the center of the Ross Archipelago (roughly at Mt. Erebus). They obtained a flexural rigidity estimate of 10^{23} N-m for the lithosphere, lower than would be expected for old, cold lithosphere (ca. 10^{24} to 10^{25} N-m). The low flexural rigidity estimate suggests the lithosphere was thermally reactivated in the Cenozoic due to heating by late volcanism and rifting following the initial Cretaceous rifting (Stern et al., 1991). Jha et al. (2013) used a semi-infinite (broken) elastic plate model to estimate the flexural rigidity of the lithosphere to be $10^{23.3}$ N-m, which agrees with estimates from Stern et al. (1991). Jha et al. (2015) completed new modeling using a semi-infinite elastic plate model and revised their original flexural rigidity estimate to 10^{21} N-m, much lower than would be expected for lithosphere of this age.

2.3 METHODS

Data gathering and synthetic seismograms

The seismic reflection data, consisting of all surveys available in the McMurdo Sound region up to the 2008 Offshore New Harbor survey, was imported into the IHS Kingdom Suite (TKS) software package for interpretation (Figure 2, Table 1). Chris Sorlien (UC Santa Barbara) provided a majority of the data. This included the BGR80, IT89, IT90, L284AN/USGS, NBP0301, NBP0306, NBP0401, NBP9601, PD90 (with permission from John Anderson, Rice University), SM87 and TH95 surveys. Additional surveys were downloaded from the Seismic Data Library System (SDLS – sdls.ogs.trieste.it) and provided by Huw Horgan (Victoria University of Wellington; HPP and MIS surveys) and Marvin Speece/Steve Pekar (Montana Tech/Queens College; ONH, ATS and MSV surveys). Navigation errors and differences in the seismic datum resulted in mis-ties in the two-way travel time to the seafloor and other distinct reflectors in many places where seismic lines intersected. This is especially problematic where the L284AN/USGS survey lines cross IT90 and NBP0401 survey lines northwest of Ross Island. The NBP0401 survey has internal mis-ties directly north of Mt. Bird, where subsea volcanic features create large seafloor relief. To fix the mis-ties associated with differences in the survey datums, static time shifts were first applied to the ONH and ATS surveys due to their close proximity to the AND-2A and CIROS-1 boreholes near Ross Island. The static time shifts were then propagated away from the boreholes by time tying the seafloor and other prominent reflectors at intersections between survey lines. Static time corrections could not be applied to correct for survey navigation errors, as the nominal line intersection does not occur at the expected location. In such instances, lines were shifted to search for a more likely intersection, and any remaining discrepancies were fixed during the contouring stage.

In order to identify key reflections in the seismic data, synthetic seismograms were created at the AND-1B, AND-2A and CIROS-1 boreholes. The synthetic seismograms allowed identification of prominent reflections that bound key stratigraphic intervals that fill the flexural moat. Correlation of the synthetic seismogram with the reflection profiles required minor adjustments in the synthetic seismograms travel times, resulting in a refined velocity profile at these 3 boreholes that is used later to convert seismic travel times to depth.

To create the synthetic seismograms, P-wave velocity (V_P) and wet-bulk density data (WBD) logs measured on the cores were downloaded from the Pangaea data repository (https://pangaea.de/; Bucker, 1998; White, 1998; Niessen et al., 2007, 2014; Dunbar, 2009) and imported into TKS. The V_P log curve was integrated to create an initial time-depth chart to convert log depths to seismic two-way travel times. This allows correlation between the core logs and the seismic data. After creating the initial time-depth chart, the V_P and WBD measurements were multiplied to generate acoustic impedance (AI) values through the depth of the borehole (Equation 1). The reflection coefficient (RC) was then calculated based on the acoustic impedance values (Equation 2).

(Equation 1) $$AI_a = V_{P_a} \times WBD_a$$

(Equation 2) $$RC = \frac{(V_{P_2} \times WBD_2) - (V_{P_1} \times WBD_1)}{(V_{P_2} \times WBD_2) + (V_{P_1} \times WBD_1)} = \frac{AI_2 - AI_1}{AI_2 + AI_1}$$

Following calculation of the AI and RC values, a synthetic seismic wavelet was generated by extracting the wavelet using frequency matching from nearby seismic traces. Frequency matching was carried out within a 1000 m search radius from the borehole, averaging approximately 70 traces per synthetic. The acoustic impedance values are then convolved with the extracted wavelet to create the synthetic seismic trace at the borehole. The synthetic trace is compared with real traces extracted from within a 500 m distance from the borehole. The well tie

is then made by shifting the entire synthetic seismogram (in time) to first align high amplitude reflectors near the seafloor on the synthetic and real traces. Then the travel time of key reflectors in the synthetic seismic trace is adjusted to match the key reflectors in the real seismic trace. Stretching and squeezing of the synthetic trace to match reflections in the real traces changes the velocity profile for the time-depth chart. This is used as a quality control. An acceptable correlation between the synthetic and real seismic traces should result in a velocity profile with realistic seismic velocities.

The seismic to synthetic seismogram ties at the three boreholes vary in quality. The tie between the AND-1B synthetic seismogram and seismic survey line MIS-1 at shot point 58 has the best fit (Figure 3). The resulting velocity profile (Figure 3, Column 2) maintains values similar to the V_P log throughout, with the highest velocity being roughly 4730 m/s at 1.804 s. All of the strong synthetic reflections match well with reflections in the real traces, especially through 1.9 s of two-way travel time. The tie between the AND-2A synthetic and seismic survey line ATS05-02 at shot point 60 has the second best synthetic to seismic fit (Figure 4). The time-depth chart velocities stay below 5000 m/s, reasonable for the rock types in this borehole (Press, 1966) and similar to the V_P log (Figure 4, Column 2). Strong reflections in the synthetic coincide with reflections in the real data (see 0.543, 0.715, 0.765, 0.791 and 1.00 s TWTT). The section between 0.6 and 0.7 s TWTT has a poor fit, where the real traces do not contain strong reflections. The final synthetic at the CIROS-1 borehole, tied to seismic survey line ONH08-01 at shot point 929, has a strong synthetic to seismic fit until 0.7 s TWTT (Figure 5). Good reflection correlations occur at the seafloor through 0.5 s TWTT (Figure 5). The time-depth chart velocities match the V_P log well (Figure 5, Column 2), except for an interval of high velocity between 0.4 and 0.5 s TWTT. Below 0.7 s TWTT, the synthetic fit is poor due to the lack of

variability in the V_P and WBD density, which results in low acoustic impedance values and small reflection coefficients.

Seismic Interpretation

Reflectors bounding strata deposited during individual flexural subsidence episodes due to volcanic loading on Ross Island were identified by the island-ward thickening wedge-shaped morphology of strata lying between them, indicating deposition due to flexural subsidence of the basin (Figure 6A, 6B, 7A, 7B). We identify two distinct reflectors, RIM-b and RIM-g, representing onlap surfaces at the base of these wedge-shaped deposits (Table 1). Two regionally extensive moat-bounding surfaces, RIB-r and RIB-m, were identified lying stratigraphically above and below the sediment packages influenced by flexure (the strata between these horizons encompass the entire flexural basin fill) (Figure 6A, 6B, 7A, 7B; Table 1). The seafloor was also mapped across the data set. After identification of key reflectors, the horizons were traced regionally across the seismic data set, verifying time ties at line intersections. Flexural fill horizons (RIM-b and RIM-g) were followed until truncating on other reflectors, identifying the depositional edge of the fill sequence. The bounding horizons (RIB-r and RIB-m) were traced across a majority of the seismic data set, well outside of the flexural basin.

Time Structure, Isochron and Isochore Maps

Time structure maps were created for all horizons by gridding the reflection travel times using the "flex gridding" algorithm in TKS (Figures 8-12). Flex gridding uses a weighted combination of minimum tension and minimum curvature gridding algorithms. Based on experimentation, the weighting was chosen to select only the minimum curvature algorithm (Briggs, 1974). The minimum curvature interpolation algorithm was chosen because it maximizes smoothness, which was deemed appropriate given the sparseness and varying spatial

density of the data. Problem areas with the computer-generated grids for RIM-b and RIM-g (indicated by unreasonably sharp changes in contour trend or slope) were corrected by hand-editing the contours to create geologically reasonable maps. The contour sets were then input into the flex gridding algorithm to generate new time grids. A final pass of hand-smoothing was applied to the contours generated from the second time grid to create the final time structure maps. The grids for the seafloor, RIB-r and RIB-m did not require hand contouring. After completing the time structure maps and ensuring they were conformable with each other and with the seismic lines, isochron maps representing the time difference between horizons were created (Figures 13-16). The isochron maps were smoothed in a manner similar to that applied to the time structure maps. To convert the isochron maps to isochore maps, interval velocities for each map were calculated at borehole AND-1B using Equation 3, where V_I is the interval velocity, Z is the thickness between horizons at the borehole (time-depth conversion was done by creating the synthetic seismogram) and TWTT is the travel time between horizons. AND-1B was chosen because it was drilled directly into the flexural moat on the southeast side of the island and is thus expected to yield the most accurate velocities in the moat, our main area of interest. The maps were smoothed as before to produce the final isochore maps (Figures 17-20).

(Equation 3) $$V_I = \frac{2*Z}{TWTT}$$

2.4 RESULTS

Seismic Stratigraphy

Four key horizons bounding strata deposited in the Ross Island flexural basin have been mapped across the data set and placed into the larger stratigraphic framework of the western Ross Sea seismic stratigraphy (Table 1). Two distinct reflectors, RIM-b and RIM-g, represent onlap surfaces at the base of wedge-shaped deposits accumulated during flexural subsidence of

the basin (Figure 6A, 6B). In addition, two regionally extensive moat-bounding surfaces were identified, RIB-m lying below the flexural strata and RIB-r above (Figure 6A, 6B).

The oldest reflector, RIB-m was traced to boreholes AND-1B, AND-2A and CIROS-1, where correlations to the synthetic seismograms indicate an age of ca. 13.57 ± 0.13 (at AND-1B, Naish et al., 2007b, Ross et al., 2012) to ~23 Ma (estimated from Wilson et al., 1998) (Figure 3-5). We assume the age of 13.57 ± 0.13 Ma to be representative for the remainder of the paper as that age was derived from reliable $^{40}Ar/^{39}Ar$ age dating of volcanics in the AND-1B borehole that was drilled into the flexural moat (Naish et al., 2007b; Ross et al., 2012). From the boreholes, RIB-m was correlated across the data set and into the VLB, where it underlies and pre-dates Ross Island and the associated flexural basin. The RIB-m reflector is laterally continuous, high amplitude, and overlies distinctively different strata imaged as a series of chaotic, parallel, moderate to high amplitude, concordant reflectors (Figures 6B, 7B).

Stratigraphically above RIB-m, reflector RIM-g is a laterally continuous, moderate to high amplitude onlap surface (Figures 6A, 7A). RIM-g was traced to borehole AND-1B, where the seismic to borehole tie suggests a rough age of ca. 4-3 Ma (Figure 3). This age range was derived from the AND-1B age model presented by Wilson et al. (2007) and Naish et al. (2007b) (Figure 3). RIM-g is present only within the flexural moat, and represents the oldest reflector associated with loading from the construction of Ross Island. At the edge of the flexural basin, RIM-g onlaps older pre-moat strata (above RIM-m). Up-section, RIM-g is onlapped by progressively younger reflectors as the onlap terminus moves away from Ross Island. The strata overlying RIM-g are low to moderate amplitude, mainly concordant reflectors that onlap underlying strata and form a thin-wedge shape that slightly thickens towards Ross Island.

RIM-b is a laterally continuous, high amplitude onlap surface similar to RIM-g. RIM-b is only present within the flexural moat, and represents the most distinct reflector associated with loading from the construction of Ross Island (Figures 6A, 7A). RIM-b was traced into the AND-1B borehole, where the seismic to synthetic tie suggests an age of <3 Ma (Naish et al., 2007b; Wilson et al., 2007), and we assume it to be ca. 2 Ma based on work by Fielding et al. (2008) (Figure 3). The horizon separates the low to moderate amplitude reflectors overlying RIM-g from more chaotic, moderate to high amplitude reflectors above that progressively onlap underlying reflectors away from the island. In cross-section, the overlying strata form a wedge-shaped deposit that thickens markedly towards Ross Island (Figures 6A, 7A). At the edge of the flexural moat, RIM-b terminates by onlapping (Figure 6B) or toplapping (Figure 7B).

The flexural fill package is capped by a younger, flat-lying seafloor-parallel reflector (RIB-r) that covers the stratigraphic wedge and conformably overlies strata outside of the flexural basin (Figures 6A, 7A). RIB-r was traced into boreholes AND-1B, AND-2A and CIROS-1, where the correlation to synthetic sesimograms suggests the age of the reflector is ca. 1 Ma (Figures 3-5). Reflectors overlying RIB-r are moderate to high amplitude, concordant and laterally discontinuous. Overlying strata are limited to the deepest portions of the basin, with the interval between RIB-r and the seafloor thinning away from Ross Island (Figure 6A).

Time Structure Maps

The RIB-m surface pre-dates formation of Ross Island. The corresponding time structure map thus captures the structure of the VLB prior to formation of Ross Island, as well as subsidence related to Ross Island (Figure 8). The TWTT for RIB-m ranges from 0.18 to 2.59 s. The dominant feature of the map is the north-south trending VLB, delineated roughly by the 1.5 s TWTT isochron (green colors, Figure 8). Structural highs are clearly visible flanking Ross

Island on the east and west sides. On the west side, the RIB-m horizon shallows rapidly as it moves onto the fault-bounded stratigraphic high known as Roberts Ridge (Figure 8), where the AND-2A, CIROS-1 and CRP boreholes were drilled. An erosional truncation was identified on the west side of Roberts Ridge. On the east side, the reflector shallows onto the flat-lying, fault-bounded Coulman High basement platform. The 1.9 s TWTT isochron (blue colors, Figure 8) show main deposition into the VLB, but a small sub-basin was identified on the north side of the map trending NNW between 166˚ and 164˚ latitude. A structural horst separates this sub-basin from the main VLB trend. The deepest part of the main VLB basin narrows dramatically south of Ross Island near the AND-1B borehole. The amount of narrowing is not well constrained due to a lack of data on the southeast side of the island, but is anchored to seismic lines near the AND-1B borehole.

The RIM-g time structure map represents the lower bounding surface of the oldest flexural basin fill, and thus marks the onset of flexural subsidence due to Ross Island volcanic loading (Figure 9). The TWTT varies from 1.13 to 2.18 s. The border of the map was delineated by the onlap extent of the horizon. On the southeast side of Ross Island, where no data exists, RIM-g was interpolated between survey lines near AND-1B (Figure 21) and the NBP0301-6A survey line on the Coulman High (Figure 22) by requiring TWTT contours to smoothly parallel the Ross Island coastline. To the north of the island the horizon does not onlap, but continues northward out of the basin with a flat-lying trend (Figure 23). The map shows a general deepening towards Ross Island (1.5 s TWTT isochron – green colors, Figure 9) from all directions superimposed on the general north-south VLB depocenter trend. The Ross Island depocenter is visible south of the island at the AND-1B borehole and surrounding seismic lines, as well as north of the island, forming a flexural moat around the island. The RIM-g horizon's

extent is strongly controlled on the west and east sides by Roberts Ridge and the Coulman High, respectively. The deepest portion of the basin (> 1.9 s TWTT), delineated by the blue shades just off the tip of Mt. Bird, is deepened by faults ("F" on Figure 9). This faulting is also responsible for the much deeper onlap observed where the -77˚ latitude line crosses the west side of the mapped area. A semi-circular structural high (< 1.45 s TWTT, red and yellow colors) is prominent north of Mt. Bird, where a volcanic feature disrupts the stratigraphy and creates relief ("V" on Figure 9; Figures 7A and 22 show the seismic line crossing the volcanic feature). The map is well constrained everywhere except for the southeast corner where the contours are interpolated to wrap and follow the island shape. However, this portion of the map is anchored at the seismic lines near AND-1B (Figure 21) and on the seismic line NBP0301-6A (Figure 22) near the Coulman High.

The RIM-b time structure map (Figure 10) represents the lower bounding surface of the upper-most wedge shaped strata package. The TWTT ranges from 1.06 to 1.97 s. The map extents were defined in the same manner as the RIM-g time structure map. Features on this map are very similar to those seen in the RIM-g time structure map. The horizon dips towards Ross Island in all directions, superimposed on the north-south trending VLB depocenter (> 1.4 s TWTT, green colors, Figure 10), forming an enclosing flexural moat. The onlap extent is controlled on the east and west sides by structural highs. On the north edge of the map, the horizon does not pinch out, but moves onto a stratigraphic high where it continues north with a flat-lying trend (Figure 23). The deepest portions of the map (> 1.8 s TWTT, blue colors), are deepened by faulting (as they were in the RIM-g time structure map) ("F" on Figure 10). The faults also cause horizon RIM-b to onlap at a larger TWTT near where the -77˚ latitude line crosses the west side of the mapped area (Figure 24). The bright semi-circular structural high (<

1.35 s TWTT, red and yellow colors, Figure 10) on the north side of the island is caused by the same volcanic center that created relief on the RIM-g map. On the southeast side of Ross Island, where no data exists, RIM-b was interpolated between the survey lines near AND-1B (Figure 21) and the NBP0301-6A (Figure 22) survey lines on the Coulman High in the same manner as RIM-g.

The RIB-r time structure map represents the upper bounding surface of the wedge-shaped strata packages (Figure 11). The TWTT ranges from 0.17 to 1.42 s. The main depocenter for this horizon forms a well-developed semi-circular moat around Ross Island (> 1.2 s TWTT, blue colors, Figure 11). To the west, the structural high known as Roberts Ridge is well defined by the map. Just north of the -77˚ latitude line, the east-west trending Mackay Sea Valley (just west of the CRP boreholes, north of latitude 77° S) is also well defined by isochrons greater than 0.9 s TWTT (green and blue colors). To the east of Ross Island, RIB-r shallows over the Coulman High, but the basin is much wider than on the RIB-m time structure map (Figure 9). Bright red and red-yellow (< 0.7 s TWTT) semi-circular features to the north of Mt. Bird delineate volcanic highs that create large relief on this horizon ("V" and "v_1" on Figure 11). Southeast of the AND-1B borehole, another red-yellow (< 0.7 s TWTT) semi-circular feature is present where the horizon shallows at it moves onto a subsea volcanic high ("v_2" on Figure 11). The map is poorly constrained to the southeast of Ross Island where there is a lack of data, but is tightly constrained elsewhere due to the widespread nature of the horizon.

The seafloor time structure map represents the modern bathymetry of the region around Ross Island (Figure 12). The two-way travel time (TWTT) varies from 0.11 to 1.29 s. The main depocenter for the seafloor currently forms a semi-circular moat around Ross Island, as in the RIB-r map. To the west of Ross Island, Roberts Ridge (< 0.5 s TWTT, red and yellow colors,

Figure 12) and the Mackay Sea Valley (> 0.8 s TWTT, blue and green colors, Figure 12) are the main features. Eastward away from the island, the seafloor gradually shallows outside the Victoria Land Basin and onto the Coulman High. Small volcanic centers create relief on the north side of the island where red to yellow (< 0.7 s TWTT) semi-circular features are present ("V", "v_1", and "v_2" on Figure 12). The area near Hut Point Peninsula, within the light gray shaded area representing the subsea edge of Ross Island, is very shallow due to the presence of subsea volcanics. The shape of the basin is well constrained along the north, west and southwest sides of the island, but poorly constrained on the southeast side of the island where there is a lack of data.

Isochron and Isochore Maps

Four isochron maps were created between RIM-g and RIM-b, RIM-b and RIB-r, RIM-g and RIB-r, and RIB-m and RIB-r (Figures 13-16). The maps were converted to thickness using interval velocities calculated at the AND-1B borehole (Figures 17-20). These maps capture, respectively, the oldest phase of flexural fill, a younger phase of flexural basin filling, the net flexural basin fill, and the broader period of basin filling in the VLB since ca. 13.57 ± 0.13 Ma (top of the RIB-m reflector).

The isochron map between RIM-g and RIM-b represents the lower-most wedge-shaped strata package (the oldest flexural basin fill) (Figure 13). The isochron values range from 0.0 to 0.25 s TWTT. The isochron (time) map was converted to an isochore (thickness) map using an interval velocity of 2178 m/s calculated from the AND-1B borehole tie. The isochore values range from 0.0 to 271 m (Figure 17). The isochore map is dominated by the N-S VLB basin trend, but shows signs of incipient flexural basin fill on the northern and southern edges of Ross Island, with overall thinning of the wedge-shaped package moving away from the island. This

interval marks the beginning of superposition of the emergent Ross Island flexural basin on the VLB trend as Ross Island began to grow. On the south side of the island, the wedge shape is thickest near AND-1B, where the flexural moat was targeted by drilling. On the north side of the island, the strata are thickest in a general north-south trend, with pronounced thickening near Ross Island. Thinning occurs (< 150 m thickness, red-yellow colors, "V" on Figure 17) in an east-west pattern in the middle of the thickest strata (> 200 m thickness, green colors, Figure 17) north of the island where the package is disrupted by a subsea volcanic center (semi-circular, red-yellow color feature on Figures 9 and 10). The thinning continues to the northwest of Mt. Bird, where the horizons are interpreted to thin over a faulted area that was difficult to interpret, and thus is not well constrained ("F" on Figure 17 and seismic profile in Figure 24). The thickening outlined by the > 200 m thick isochore (green colors, Figure 17) north of the island is disrupted by what are likely artifacts that resulted from differences in interpolation of the time structure maps.

The isochron map between RIM-b and RIB-r represents the upper wedge-shaped strata package (Figure 14). The isochron values range between 0.01 and 0.71 s. The isochron map was converted to thickness using a calculated interval velocity from the AND-1B borehole tie of 2328 m/s. The isochore thicknesses range from 10 to 830 m (Figure 18). The isochore map highlights the main flexural basin and indicates that the basin at this time was deepest north of the island (> 600 m thickness, green colors, Figure 18). The strata thicken towards Ross Island, as would be expected for the volcanic loading as the island was continuing to erupt. The wedge near borehole AND-1B is much thinner than the wedge north of the island, implying the borehole may have targeted a shallow portion of the flexural basin. North of the island, the thickest portions of the map lie slightly northeast of Mt. Bird where thickness values are greater

than 650 m due to disruption by a volcanic feature ("V" on Figure 18). Northwest of Mt. Bird is deepened by faulting ("F" on Figure 18).

The isochron map between RIM-g and RIB-r encompasses the entire flexural basin fill, from onset through deposition of both wedge-shaped strata packages (Figure 15). The isochron map values range from 0.0 to 0.99 s. The isochron map was converted to an isochore map using a calculated interval velocity of 2281 m/s from the AND-1B borehole. The isochore thickness ranges from 0 to 1110 m (Figure 19). The isochore map looks similar to the isochore between RIM-b and RIM-r (Figure 18), in that the main flexural basin is located north of the island with a north-south trend. There is also a general increase in thickness towards Ross Island. Volcanism northeast of Mt. Bird thickened the isochore map between these horizons ("V" on Figure 19). Just as in the previous isochore map, the strata near AND-1B are part of the flexural moat, but are not located in the thickest portion of the basin. Some thinning of the flexural strata also occurs northwest of the island, where younger faulting created relief in the subsurface and shallowed RIM-g ("F" on Figure 19 and seismic profile in Figure 24). Overall, the entire flexural basin is well defined by this stratigraphic interval.

The isochron map between bounding horizons RIB-m and RIB-r highlights the overall depositional patterns that began prior to the formation of Ross Island and those which followed filling of the flexural moat (Figure 16). The isochron values range from 0.0 to 1.72. The isochron map was converted to thickness using a calculated interval velocity of 2535 m/s from the AND-1B borehole. The isochore thickness ranges from 0 to 2114 m (Figure 20). The map shows the VLB depocenter of pre-Ross Island times combined with the flexural basin that developed in conjunction with the formation of Ross Island formed. The red colors (~ 700-900 m thickness isochores, Figure 20) near Ross Island roughly bound the north-south trend of the VLB that is

evident in the RIB-m time structure map (Figure 8). The green and blue colors (> 1100 m thickness isochores) roughly bound the flexural basin near the AND-1B borehole and north of the island near Mt. Bird. Features seen in the RIB-m time structure map are evident in the RIB-m/RIB-r isochore map, such as the NNW trending sub-basin in the northwest corner of the map (> 1100 m thickness, green colors) and the structural high just east of that sub-basin (< 900 m thickness, yellows and red colors). The semi-circular dark blue (> 1850 m thickness) colored feature north of Ross Island is the result of a volcanic feature creating relief on the RIB-r horizon without uplifting the RIB-m horizon ("V" on Figure 20). The thinnest portions of the map lie on the structural highs on the east and west sides of Ross Island, where the horizons shallow and strata within the flexural basin fill have pinched out. The main depocenter has a north-south trend, with the thickest strata on the north and south sides of the island, north of Mt. Bird and near AND-1B, respectively. The main depocenter narrows on the south side of the island, although the position and amount of narrowing is poorly constrained due to a lack of data southeast of the island.

2.5 DISCUSSION

Evolution of the Ross Island Flexural Moat

Seismic reflection surveys and borehole data provide a picture of the Ross Island flexural moat evolution since ca. 13.57 ± 0.13 Ma, beginning with deposition of the RIB-m horizon. At 13.57 ± 0.13 Ma, prior to formation of Ross Island and the flexural moat, the pre-moat strata were deposited in the large, N-S trending Victoria Land Basin depocenter (Figure 8). The VLB depocenter is sharply controlled by fault-bounded structural highs, the Coulman High to the east and Roberts Ridge to the west (Figure 8). The VLB depocenter narrows abruptly to the south below Ross Island and the Ross Ice Shelf. There is no evidence of further VLB or Terror Rift

subsidence following deposition of the RIB-m reflector. Instead, younger sediments filled the N-S depocenter trend until Ross Island began to form ca. 4.6 Ma with the emergence of Mt. Bird (Armstrong, 1978; Esser et al., 2004).

As Ross Island grew and volcanically loaded the crust, the lithosphere responded by flexural down-warping. This down-warping is evident in horizon RIB-g, the first horizon interpreted to be flexurally influenced by volcanic loading (Early Pliocene age, ca. 4-3 Ma based on Naish et al., 2007b and Wilson et al., 2007 age dates). The incipient flexural moat is evident in the RIM-g/RIM-b isochore (Figure 17), where the emergent flexural moat is superimposed on the N-S VLB/Terror Rift trend. The moat is filled with a wedge-shaped strata package between RIM-g and RIM-b that thickens by up to~260 m towards Ross Island, with younger reflectors onlapping up-dip onto RIM-g (Figure 6B, 7B). The depocenter of the moat at this time is located mainly north and northeast of Mt. Bird, where fault deepening (possibly related to the Terror Rift), subsea magmatic intrusions/extrusions, and flexural subsidence combine to form the composite basin (Figure 17).

Further growth of Ross Island loaded the crust and caused additional flexure and basin filling, evident from the RIM-b/RIB-r isochore map (Figure 18). Evidence for a second phase of flexure includes the presence of a new onlap surface (RIM-b), a change in the seismic stratigraphic character, from chaotic, low amplitude strata below RIM-b to concordant high amplitude strata and development of a wedge-shaped strata package (Figure 6A, 6B). The stratigraphic wedge lying between RIM-b and RIB-r thickens up to ~ 850 m from the east and west sides towards Ross Island, forming an enclosing flexural moat (Figure 18). Progressive onlapping of younger strata onto RIM-b occurs moving away from the island (Figure 6B, 7B). The main depocenter follows the island coastline, with the deepest portion located offshore

northeast of Mt. Bird, where faulting (possibly related to the Terror Rift), magmatism and flexural subsidence have affected the basin and basin-fill strata (Figures 7A, 7B, 18, and 25). The superposition of the flexural moat over the N-S VLB/Terror Rift trend is still apparent as the flexural moat is filled (Figure 18) and then subsequently covered by RIB-r (Figure 6A, 7A).

RIB-r was deposited as the cap to wedge-shaped strata filling the flexural moat since the incipient flexural moat was formed ca. 4 Ma (Figure 6A, 7A). The RIM-g to RIB-r isochore encompasses the entire flexural basin fill, up to ~1.1 km of strata (Figure 19). The map suggests the enclosing flexural moat is present around the entire island, but narrow on the west side due to the presence of Roberts Ridge and magmatism near Hut Point Peninsula. The moat follows the shape of the island on the south side near AND-1B and on the southeast side below the Ross Ice Shelf. On the north side, the main depocenter is superimposed on the N-S trend of the underlying VLB/Terror Rift basin, suggesting the underlying structures influenced the extent of the flexural basin. Faulting and volcanic features north of the island complicate the depth of the depocenter to the northeast of Mt. Bird, where the basin-fill strata thicken and thin over magmatic highs and faults in the subsurface (Figure 19). Deposition of the RIB-r horizon extends beyond the flexural moat, where the horizon conformably overlies strata over the structural highs and throughout the mapped area (Figure 11). This horizon represents the first preserved strata that were deposited outside of the flexural basin since the moat was formed ca. 4 Ma.

The position of the primary flexural moat depocenter is north of the island (Figure 19). The cause of the northward shift of the primary Ross Island flexural basin depocenter is unclear. McMurdo Volcanic Group volcanic centers present north of the island are straddled by wedges of sediment indicating flexural subsidence in response to a northward shifted load (Figure 7A). However, these features are also seen uplifting the flexural basin fill strata, implying the load

may be deeper in the stratigraphy (Figure 7A). Alternatively, high temperatures and molten or partially molten rock beneath Mt. Erebus may contribute a negatively buoyant load directly beneath the island, shifting the load center of mass northward. Finally, the northward shifted depocenter could be explained as an artifact resulting from a seaward-thickening wedge of shelf sediment derived from the Ross Ice Shelf on the south side of Ross Island and deposited into the VLB/Ross Island flexural moat depocenters.

Two packages of flexure-related fill were identified and mapped (represented by the RIM-g/RIM-b and RIM-b/RIB-r isochore maps). The oldest fill (Figure 17), here termed Unit FFI was deposited above RIM-g, from ca. 4 Ma to ca. 2 Ma (derived from age models at the AND-1B borehole), during the time of crustal loading as Mt. Bird grew (Armstrong, 1978; Esser et al., 2004). The AND-1B borehole recovered four lithostratigraphic units (LSU) of this age that can be used to define the strata in the FFI flexural fill interval (all lithostratigraphic units are from Krissek et al., 2007). LSU 4.1, the oldest lithostratigraphic unit, consists of diatomite that was overlain by LSU 3.6, a biosiliceous-rich diatomite, mudstone and diamictite layer. LSU 3.5 was deposited as an interval of silty claystone, sandstone and muddy diamictite. Finally, LSU 3.4, a biosiliceous-bearing diamictite was deposited as flexural strata overlying RIM-g gave way to RIM-b. Overlying RIM-b is the youngest flexural basin fill, Unit FFII. Unit FFII was deposited from ca. 2 Ma to ca. 1 Ma during the time of crustal loading by Mt. Terror, early eruptions of Mt. Erebus, and Hut Point Peninsula (Armstrong, 1978; Esser et al., 2004). This time period covers five lithostratigraphic units described from the AND-1B borehole (Krissek et al., 2007). From oldest to youngest – LSU 3.3 consists of alternating diamictite and diatomite; LSU 3.2 is a silty claystone and mudstone alternating with diatomite; LSU 3.1 is a muddy

diamictite with diatomite; LSU 2.4 is a volcanic sandstone, siltstone and mudstone; and finally LSU 2.3 is a diamictite, volcanic sandstone and silty claystone (Krissek et al., 2007).

The lithostratigraphic units filling the flexural basins support the idea of two distinct phases of flexure and sediment filling. As flexural loading and down-warp occurred, original deposition into FFI consisted of low-energy hemipelagic or pelagic sedimentation of siliceous diatomaceous ooze into the flexural moat, coincident with emergence of Mt. Bird eruptions. Additional low-energy sediment deposition followed the Mt. Bird emergence, when mudstones and diatomites were deposited together, likely as pelagic sediment. As the basin filled, coarser grained sediments were deposited as diamictite, silty claystone, sandstone and muddy diamictite into the flexural basin, possibly derived from the ice sheet to the south (diamictite) and the Transantarctic Mountain front to the west (siliciclastics, see downlapping patterns in Figure 6B and 7B). Additional diamictite was deposited at the interface between FFI and FFII as the first flexural basin was filled, and flexural subsidence down-warped the basin.

The lower interval of FFII is dominated by the diamictite layer associated with FFI over-filling, until ice sheet waxing and waning led to alternating deposition of diamictite and pelagic diatomite. The diatomite deposition is theorized to be coincident with additional volcanic activity as Ross Island grew, producing a submarine environment high in biological productivity. Silty claystone and mudstone, alternating with diatomite represent deposition of TAM-derived sediment intermixed with periods of biologic productivity. A period of ice-sheet waxing and waning complicated the filled of the second flexural sub-basin as muddy diamictite and diatomite alternate. As the flexural basin was filled, volcaniclastic sandstone, likely shed off Ross Island, was deposited into the flexural basin along with TAM-derived siliciclastics. The flexural basin continued to fill with siliciclastics before ice sheet growth resulted in the

deposition of diamictite, followed by additional volcaniclastic sandstone deposition as the ice sheet receded. The final cap to the flexural basin fill was a subglacial silty-claystone layer, deposited pelagically and conformably covering the entire flexural basin fill as horizon RIB-r. Above horizon RIB-r lays is a thin, possibly flexurally influenced wedge of strata overlain by the modern seafloor (Figure 6B). If this wedge is indeed flexural, it would indicate that subsidence of the flexural moat is ongoing today.

Basin filling was likely the result of rapid post-flexural deposition. Both FFI and FFII have distinct stacking patterns characterized by their wedge-shaped geometry, progressive up-dip onlap away from Ross Island and downlap towards Ross Island. The progressive up-dip onlap away from Ross Island suggests that the flexural moat was filled quickly. The island-ward downlapping indicates sediment was supplied down the slope, possibly by mass flow or pelagic sedimentation (Figure 6B). Above RIM-b, some of the strata near the top of the fill downlap away from the island, indicating they were derived from the island edge (Figure 6B). These two sediment packages are distinguished by their distinct onlap surfaces, the horizons RIM-g and RIM-b. Horizons within both of the flexural wedges are generally parallel and do not diverge in the direction of the island, indicating deposition following flexural down-warping rather than growth strata deposited as the basin subsided (Figure 26). The seismic stratigraphy suggests that the flexural basin was filled from sediment derived from both the island and the slopes to the east and west. The basin filling patterns show that horizon RIM-g has a slightly wider extent than horizon RIM-b, indicating either a reduction in sediment supply, or weakening of the lithosphere over time, causing the flexural basin to narrow (Figure 9, 10, and 26).

Basin filling patterns on the north side of Ross Island are complicated by the presence of intrusive and extrusive magmatic features (Figure 7A and 25). The RIB-m surface represents the

basin prior to flexural subsidence. Volcanic features do not uplift the RIB-m horizon, and thus are interpreted to have been built on top of the RIB-m surface (Figure 8). The time structure maps for the RIB-r, RIM-g and RIM-b all show uplift over the volcanic features northeast of the island (Figure 8, 9, and 10). The RIM-g/RIB-r isochore (Figure 19) clearly shows thickening northeast of Mt. Bird, where magmatic activity uplifted the deeper flexural basin fill strata (Figure 7A and 25). This magmatic activity post-dated the initial filling of the flexural basin, as the flexural strata has been disturbed and uplifted (Figure 7A and 25). The isochore maps for the intervals between the flexural horizons (RIM-g and RIM-b) and RIB-r (Figures 18 and 19) show a thickening of the sequence over this volcanic feature. A possible explanation for this thickening is that extrusive volcanic eruptions in this area added overlying material to the basin-fill strata prior to deposition of the capping horizon, RIB-r (Figure 7A and 25). The RIB-r and seafloor time structure maps both show this volcanic feature, indicating it has been active at least up until deposition of the modern seafloor.

There is no seismic evidence that ice grounding events scoured or re-worked sediments within proximal parts of the flexural basin (e.g., on seismic line NBP0401-126m; Figure 6A and 6B). However, evidence of glacial scouring in this area has been identified in stratigraphy immediately below the flexural basin fill (Figure 6B). The lack of scour marks within the strata filling the flexural basin suggests that Ross Island volcanic loading coincided with the end of ice grounding events within proximal parts of the flexural basin. We infer the lack of ice grounding events was caused by the flexural subsidence of the lithosphere to support the Ross Island load. The end of ice grounding due to flexural subsidence effectively de-coupled the stratigraphic record contained in the proximal basin from the sedimentary climate record and the effects of regional tectonics. This de-coupling occurred after the main Victoria Land Basin tectonic phase,

during the thermal subsidence phase of the basin. It is worth noting that the AND-1B borehole, located in the distal part of the flexural basin south of Ross Island and subject to less flexural subsidence, shows evidence of ice grounding during the Plio-Pleistocene (Naish et al., 2007b).

2.6 SUMMARY

This thesis presents the first maps that illustrate the complete evolution of the Ross Island flexural moat from the background deposition ca. 13 Ma through formation of the moat and cessation of flexural subsidence ca. 1 Ma. Marine and over-ice multi-channel seismic reflection surveys and borehole studies completed over the last 30+ years were used to identify and map stratigraphy that bounds and fills the Ross Island flexural basin. The seismic data provide adequate coverage on the north, west, and south sides of the island to confidently identify and map the basin fill stratigraphy. The east (and especially southeast) side of the island lacks seismic data to constrain the flexural basin strata, but interpretive contouring anchored to seismic lines over the Coulman High and near the AND-1B borehole allows complete interpolation of the flexural basin map around Ross Island. Four key stratigraphic horizons were identified and mapped (Table 1) to fully capture the spatial and temporal evolution of the flexural moat. Horizon RIB-m (ca. 13 Ma) was deposited prior to formation of Ross Island within the N-S trending Victoria Land Basin depocenter. RIB-m extends throughout the basin and onto structural highs to the east and west, known as the Coulman High and Roberts Ridge, respectively. Horizon RIM-g (ca. 4 Ma) is an onlap surface interpreted to represent the lowest surface bounding the flexural basin fill. Horizon RIM-b (ca. 2 Ma) is interpreted to represent a second onlap surface that captures a second period of basin filling. Horizon RIB-r (ca. 1 Ma) was deposited as a flat-lying cap to the flexural basin strata that conformably overlies strata outside of the flexural basin.

The stratigraphic maps show that the Ross Island flexural moat first began to form ca. 4 Ma, with deposition of the RIM-g horizon as Mt. Bird was emerging. Two distinct periods of flexural subsidence and sedimentation are evident, described above as units FFI and FFII, associated with the growth of Mt. Bird (FFI ca. 4 Ma to 2 Ma) and Mt. Terror, Mt. Erebus and Hut Point Peninsula (FFII ca. 2 Ma to 1 Ma). These two periods of flexural subsidence and post-flexural deposition are characterized by distinct wedges of strata that thicken towards Ross Island and onlap patterns moving progressively up-dip away from the island. Periods of flexural subsidence are separated by tectonically quiescent basin-filling punctuated by deposition of diamictite and diatomite from the waxing and waning of ice sheets. The flexural moat is superimposed on the N-S trending VLB depocenter, reaching a total estimated thickness of approximately 1.1 km north of Ross Island, with a shallower moat (~ 400 m thickness on average) enclosing the entire island. The deepest part of the basin is located north of Ross Island, rather than below the presumed primary topographic load. The cause for the northern location of the primary depocenter is unclear. Hypotheses for factors contributing the depocenter location include: i) volcanic loading by McMurdo Volcanic Group subsea volcanic features north of the island, ii) partial compensation of the main Ross Island load by low-density, partially molten rock beneath the island, iii) extensional faulting within the Terror Rift, or iv) seaward-thickening wedge of shelf sediments derived from the Ross Ice Shelf and deposited into the VLB/Ross Island flexural moat depocenters. The seismic data show that the onset of filling of the flexural moat around Ross Island coincided with the end of ice grounding events in the proximal areas of the moat. We infer that this was caused by flexural subsidence of the seafloor to accommodate the Ross Island load.

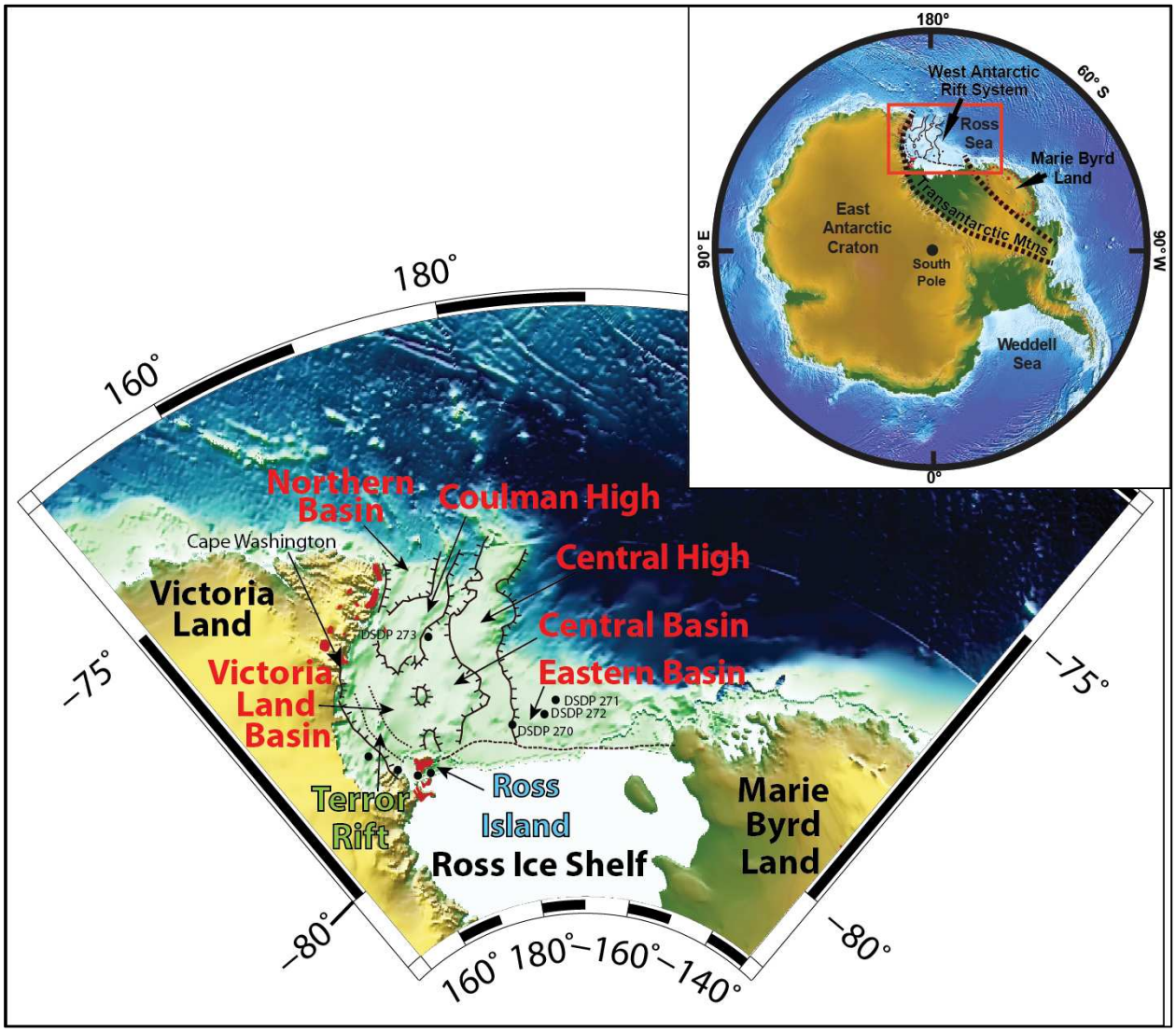

Figure 1. Location map of the Ross Sea region and its location on the Antarctic continent (inset). Major tectonic (WARS related) and geographic features are labeled. Volcanic features are shaded red. Black dots represent boreholes.

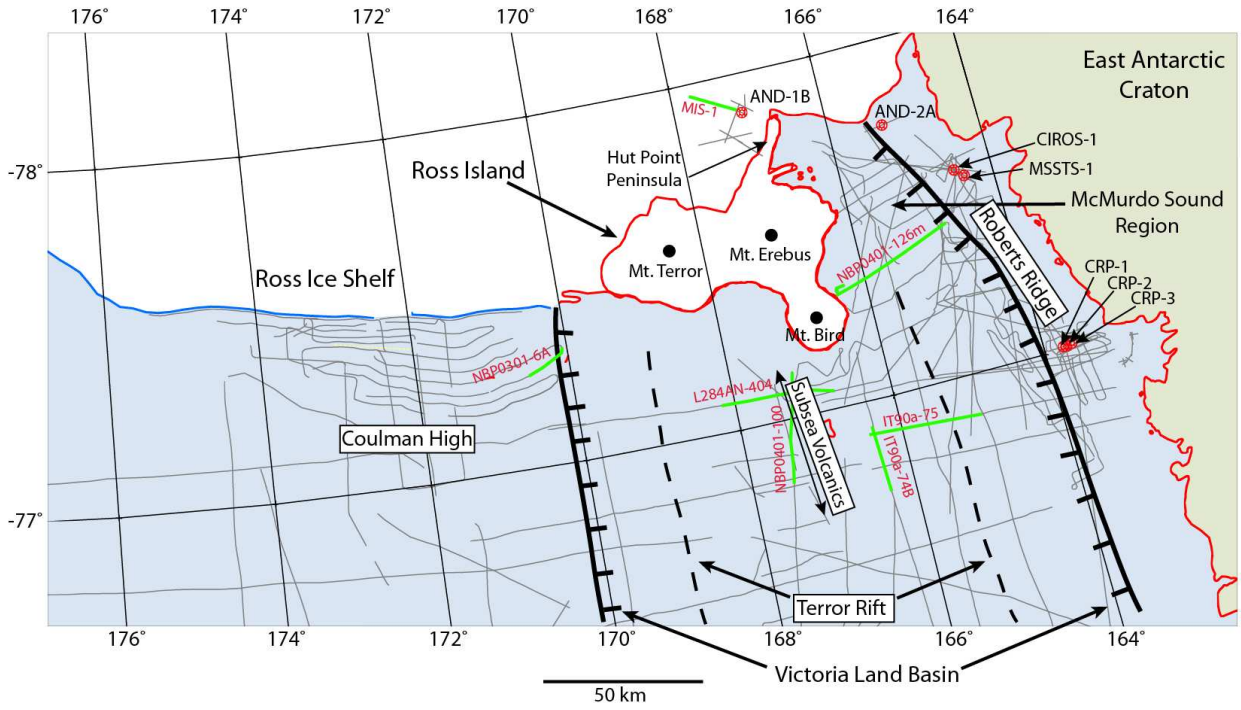

Figure 2. Seismic base map of the area around Ross Island (island and coastline outlined in red, blue line denotes edge of ice shelf), showing all seismic lines (light gray or green highlighted lines) and boreholes (red dots) in the region. Green highlighted seismic lines are labeled with their names and will be presented in the paper. Blue shaded region represents water, white shaded represents the Ross Ice Shelf, and green shaded region represents the East Antarctic Craton.

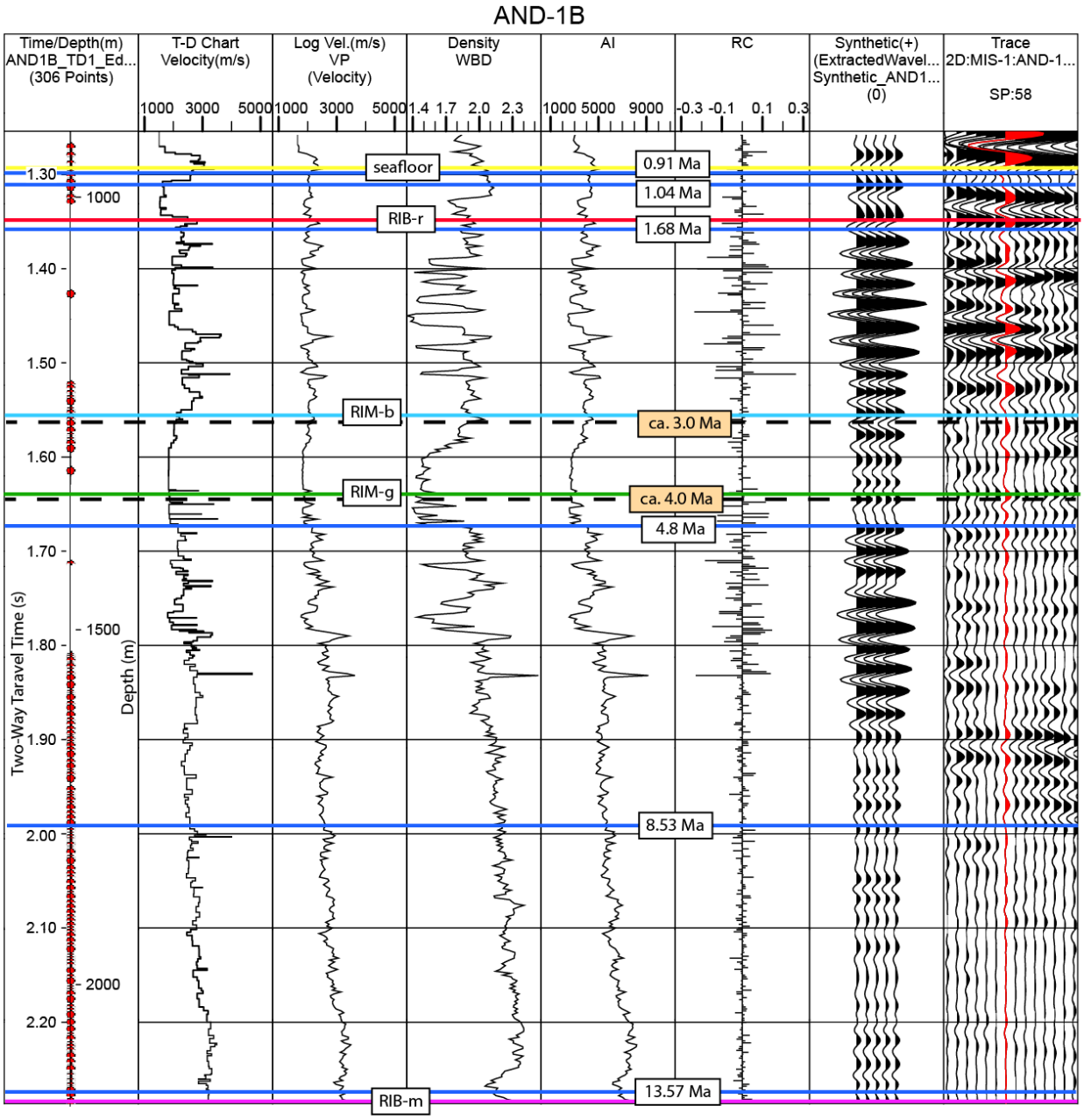

Figure 3. Synthetic seismogram at the AND-1B borehole. Column 1: Time-depth (T-D) chart. Red dots represent measured travel time from the borehole. Column 2: Time-depth chart velocity. Column 3: P-wave velocity log. Column 4: Wet-bulk density log. Column 5: Acoustic Impedance. Column 6: Reflection Coefficient. Column 7: Synthetic traces (5 traces repeated for ease of viewing). Column 8: Real traces from seismic line MIS-1. SP = shot point at which the borehole intersects the seismic line. Thin blue lines represent the ages from Ross et al. (2012). Colored lines indicate horizons mapped in this study. Dashed lines with filled boxes (peach filled) represent approximate ages from Figure 2 of Naish et al. (2007b) and Wilson et al. (2007). The reflectors from this study correspond to those presented by Fielding et al. (2008): RIB-r = Rk, RIM-b, = Rj, RIB-m = Rg (Table 1).

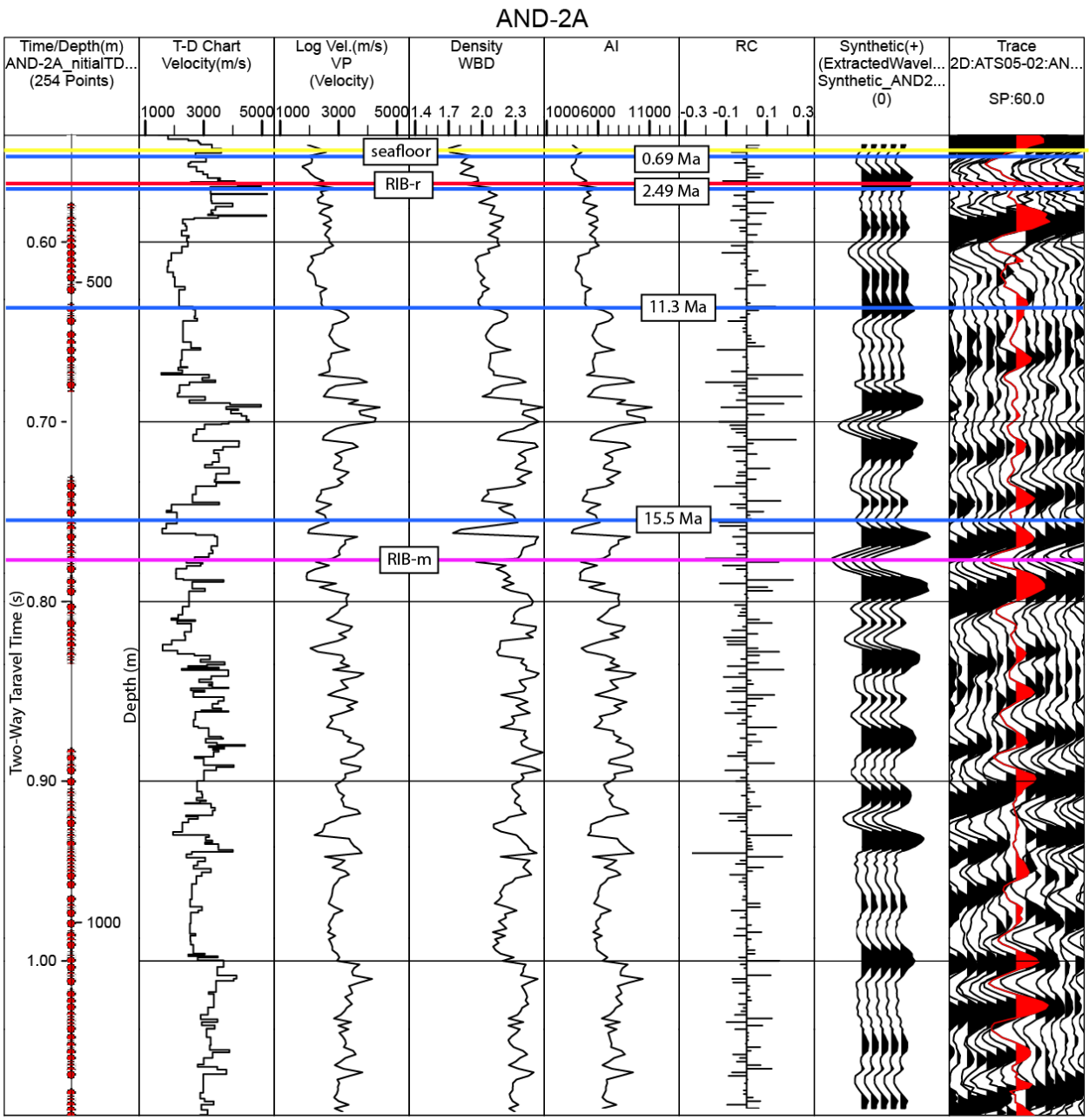

Figure 4. Synthetic seismogram at the AND-2A borehole. Column 1: Time-depth chart. Column 2: Time-depth chart velocity. Column 3: P-wave velocity log. Column 4: Wet-bulk density log. Column 5: Acoustic Impedance. Column 6: Reflection Coefficient. Column 7: Synthetic traces (5 traces repeated for ease of viewing). Column 8: Real traces from seismic line ATS05-02. SP = shot point at which the borehole intersects the seismic line. Thin blue lines represent the ages from Table 1 of Acton et al. (2008). Colored lines indicate horizons mapped in this study.

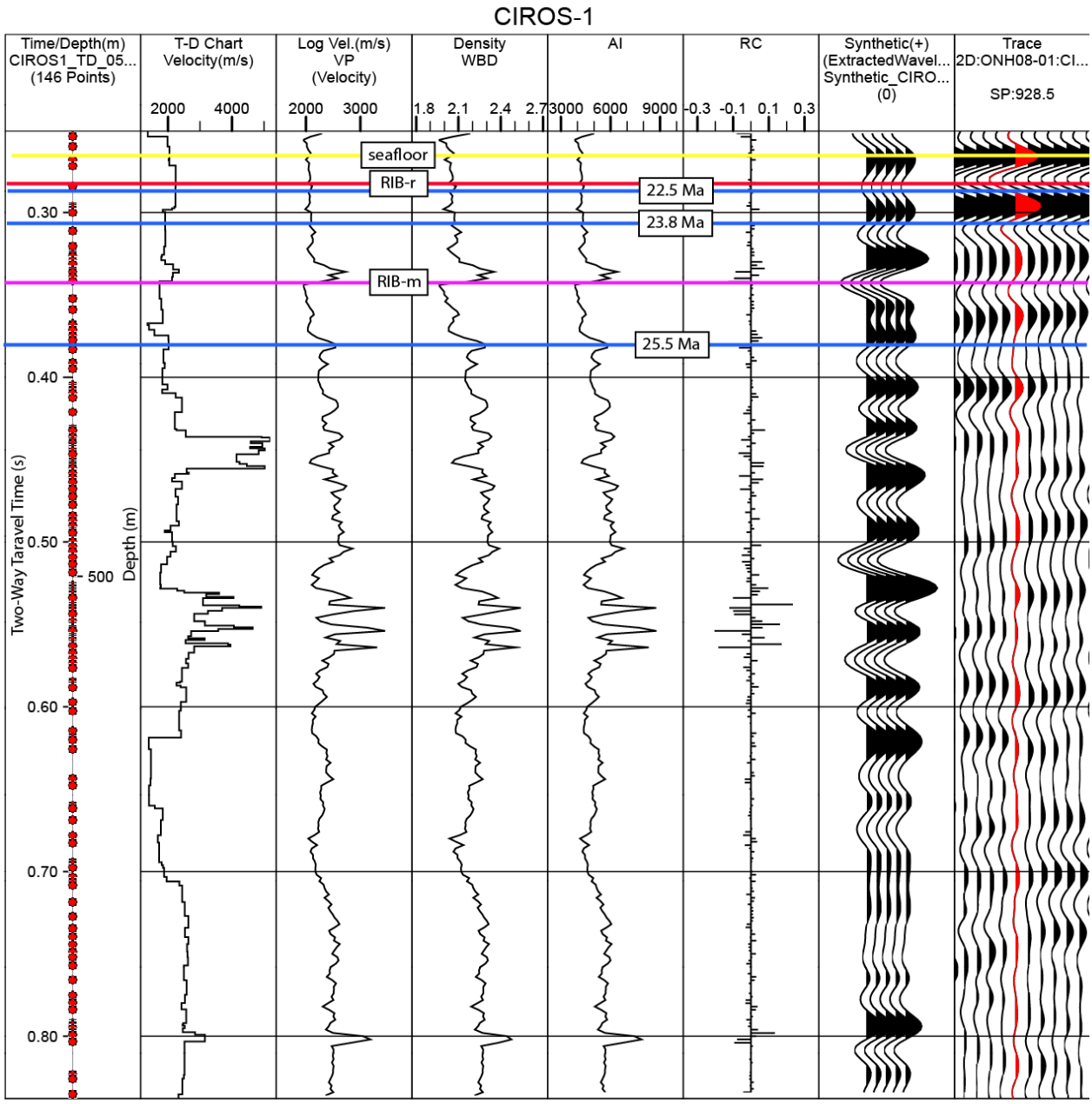

Figure 5. Synthetic seismogram at the AND-1B borehole. Column 1: Time-depth chart. Column 2: Time-depth chart velocity. Column 3: P-wave velocity log. Column 4: Wet-bulk density log. Column 5: Acoustic Impedance. Column 6: Reflection Coefficient. Column 7: Synthetic traces (5 traces repeated for ease of viewing). Column 8: Real traces from seismic line ONH08-01. SP = shot point at which the borehole intersects the seismic line. Thin blue lines represent the ages from Table 1 of Harwood et al. (1989). Colored lines indicate horizons mapped in this study.

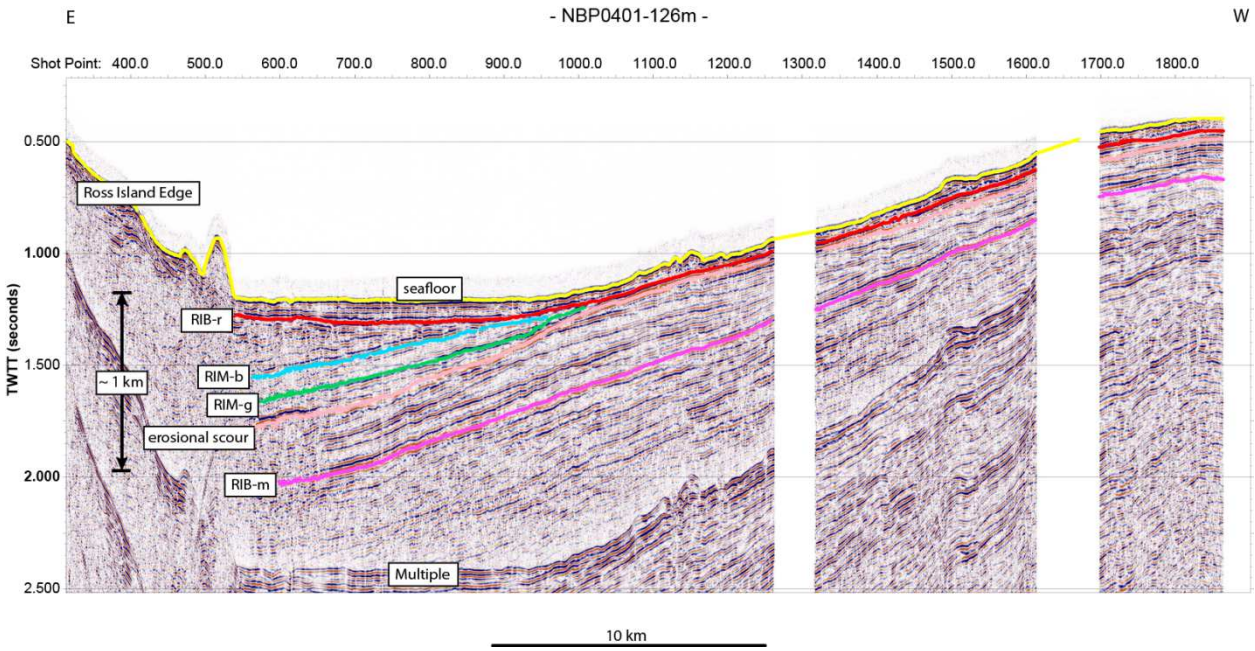

Figure 6A. Seismic reflection dip line NBP0401-126m (see Figure 2 for location) showing the picked horizons. This line highlights the overall pattern of deposition in the VLB, as well as the filling of the flexural basin beginning at the RIM-g reflector (see Figure 6B for a closer view of the flexural basin fill). The conformable nature of the bounding horizons RIB-r and RIB-m is easily identifiable moving west out of the flexural basin.

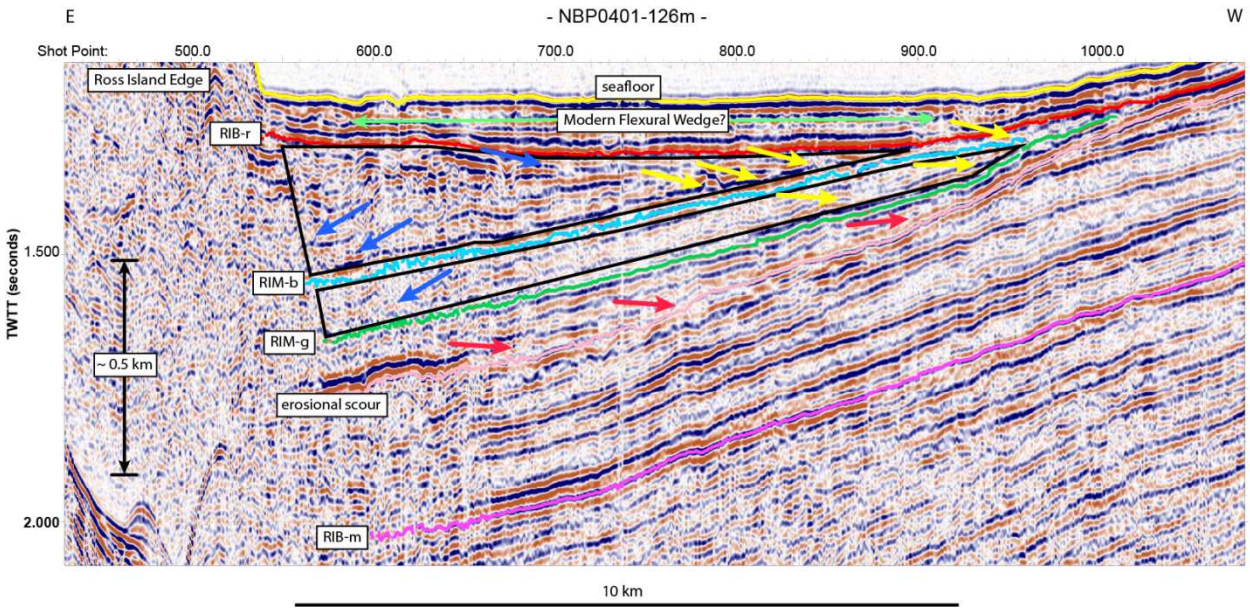

Figure 6B. The portion of seismic reflection dip line NBP0401-126m that has been affected by flexure (entire basin-fill from RIM-g to RIB-r). Black triangles outline flexural basin wedge-shaped strata packages. Yellow arrows emphasize onlap patterns in the basin-fill strata. Red arrows highlight a wedge-shaped strata package below RIM-g that onlaps an erosional scour surface. Blue arrows indicate direction of sediment supply associated with respective downlap patterns.

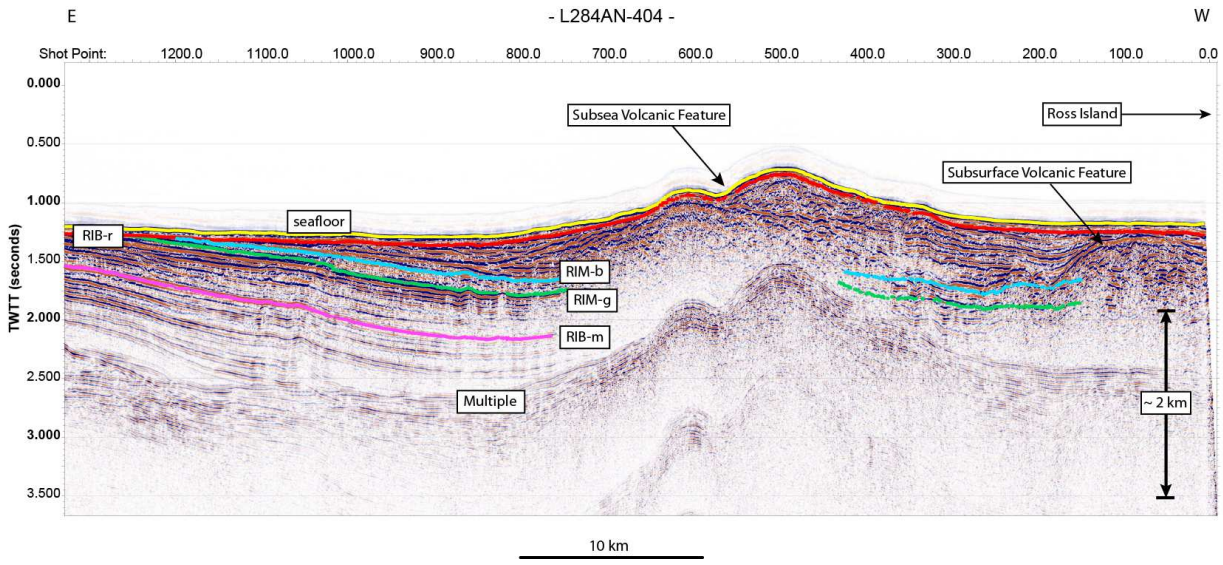

Figure 7A. Seismic reflection dip line L284AN-404 (see Figure 2 for location) highlighting the presence of the flexural basin on the east side of Ross Island. Subsea and subsurface volcanic features are evident in this line.

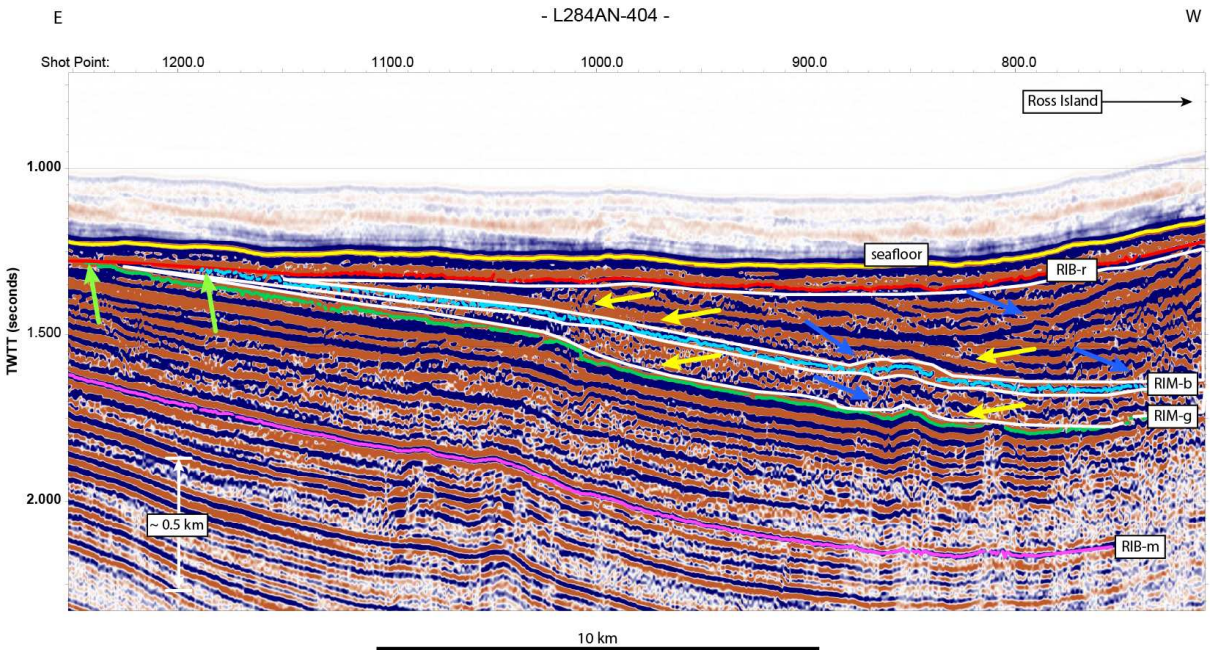

Figure 7B. The portion of seismic reflection dip line L284AN-404 that has been affected by flexure. White triangles outline flexural basin fill packages. Yellow arrows emphasize the onlap patterns within the flexural strata. Blue arrows indicate direction of sediment supply associated with respective downlap patterns. Green arrows indicate toplap.

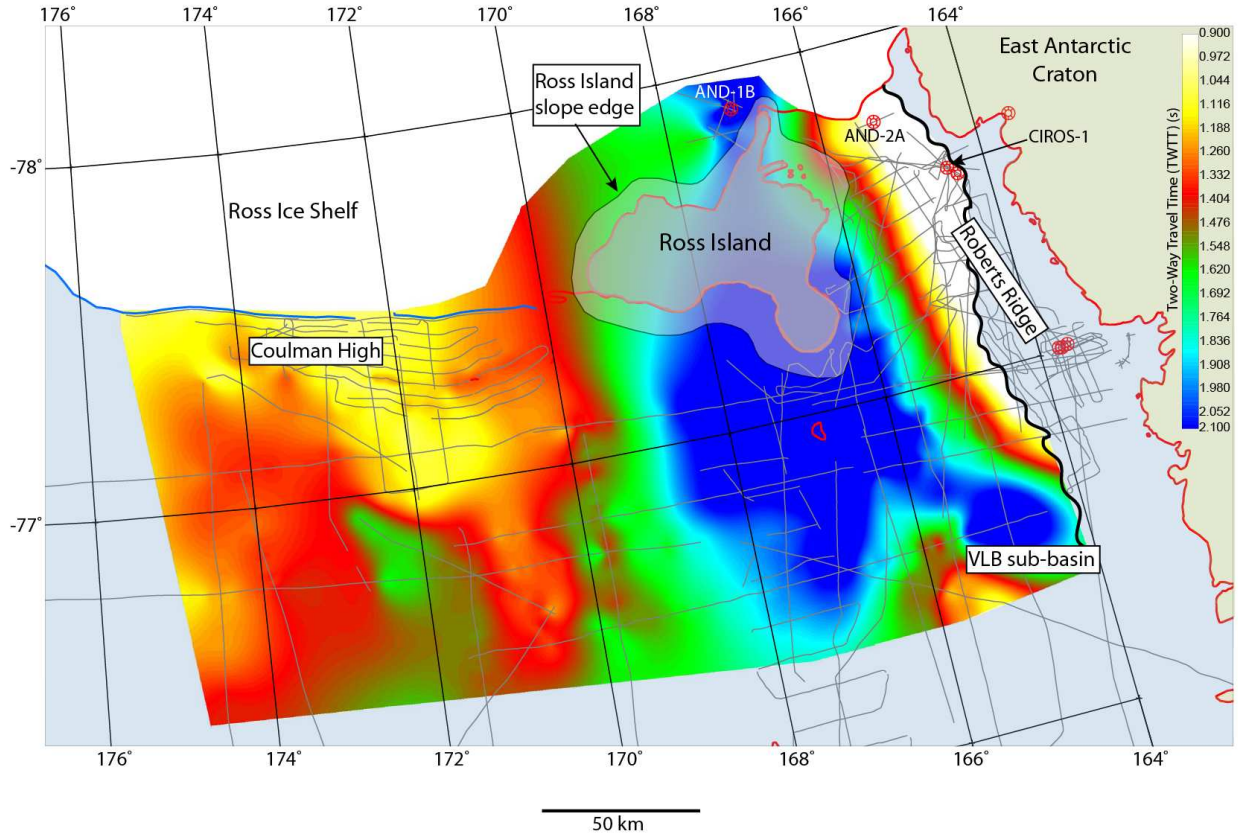

Figure 8. Time structure map of horizon RIB-m. This horizon represents the youngest strata presenting the Victoria Land Basin prior to formation of Ross Island. The light gray outline surrounding Ross Island represents the edge of the Ross Island volcanic pile. The black, wavy line on the west side of the map represents the approximate location of an unconformity where the RIB-m horizon was eroded.

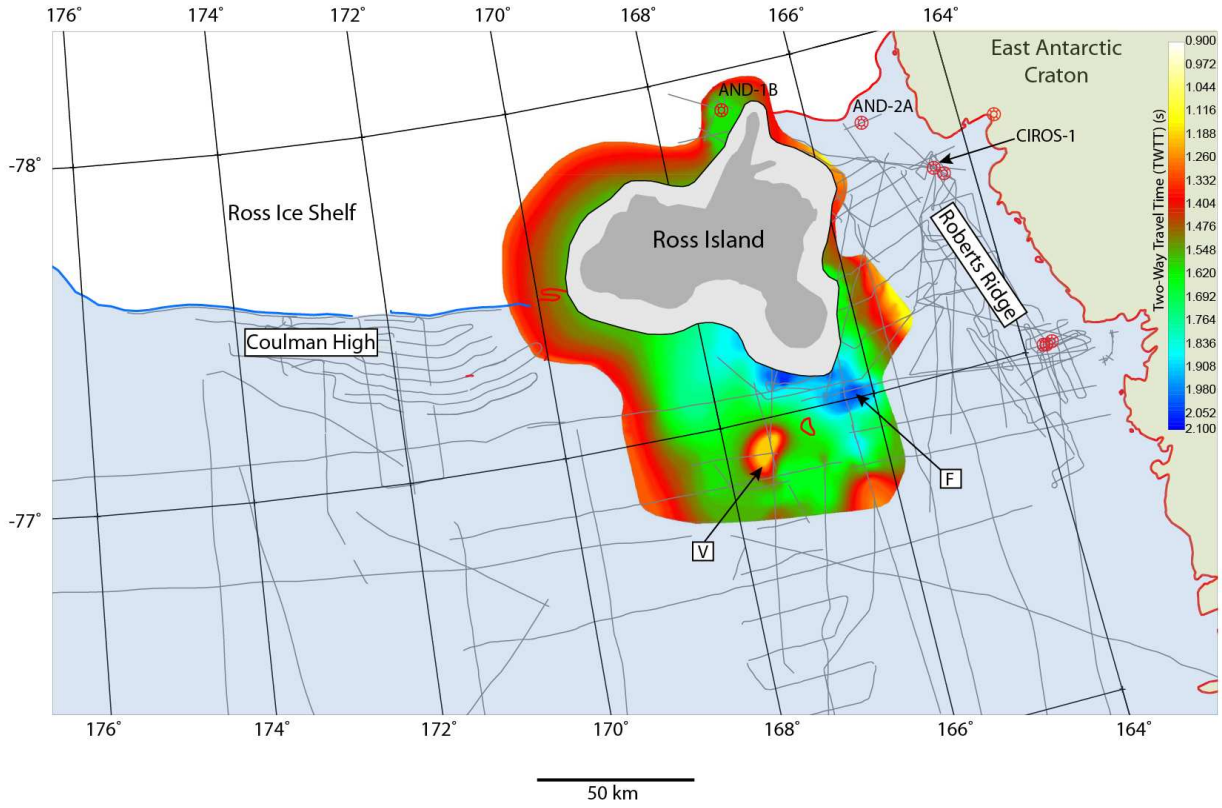

Figure 9. Time structure map of the RIM-g horizon. This horizon represents the lower bounding surface of the oldest flexural strata around Ross Island. The light gray outline surrounding Ross Island represents the edge of the Ross Island volcanic pile. Letters indicate features discussed in the text (V = volcanically disrupted area, F = fault-disrupted area).

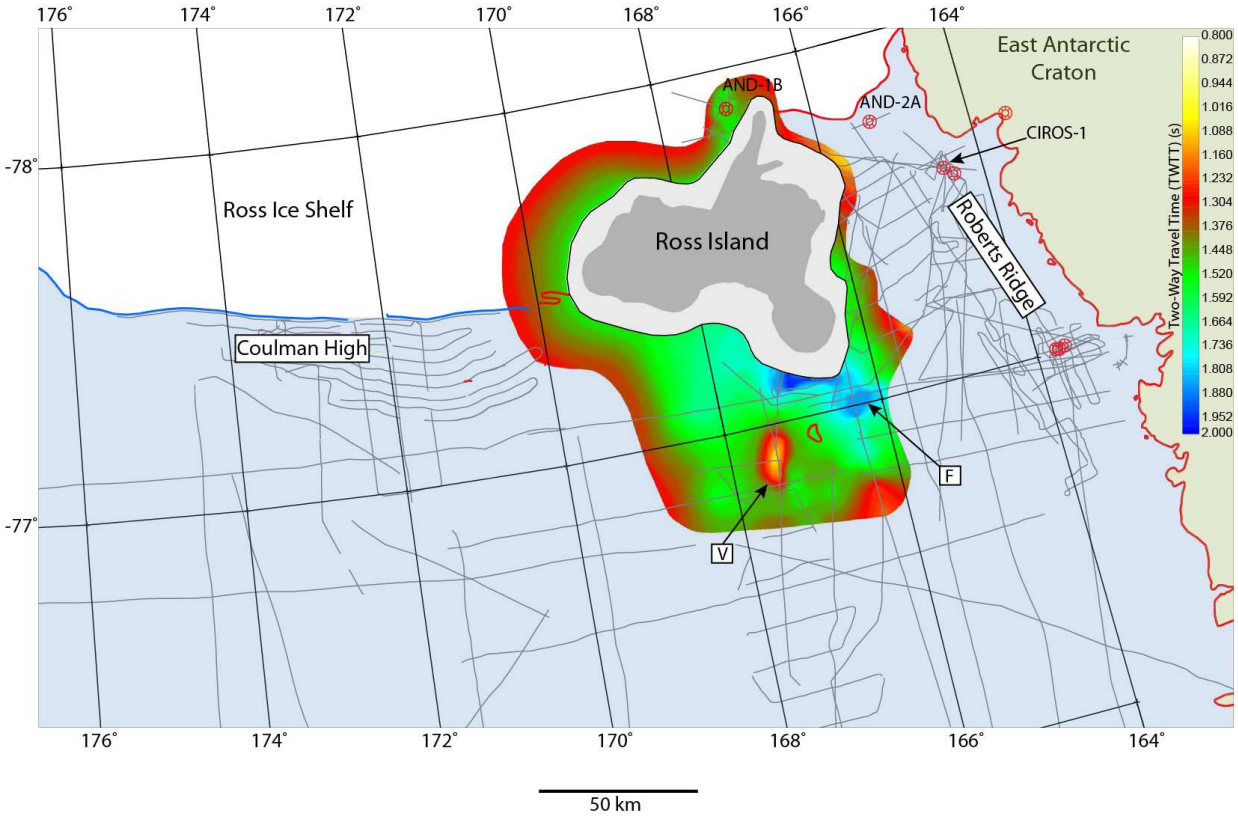

Figure 10. Time structure map of the RIM-b horizon, the lower bounding surface of the youngest flexural strata around Ross Island. The light gray outline surrounding Ross Island represents the edge of the Ross Island volcanic pile. Letters indicate features discussed in the text (V = volcanically disrupted area, F = fault-disrupted area).

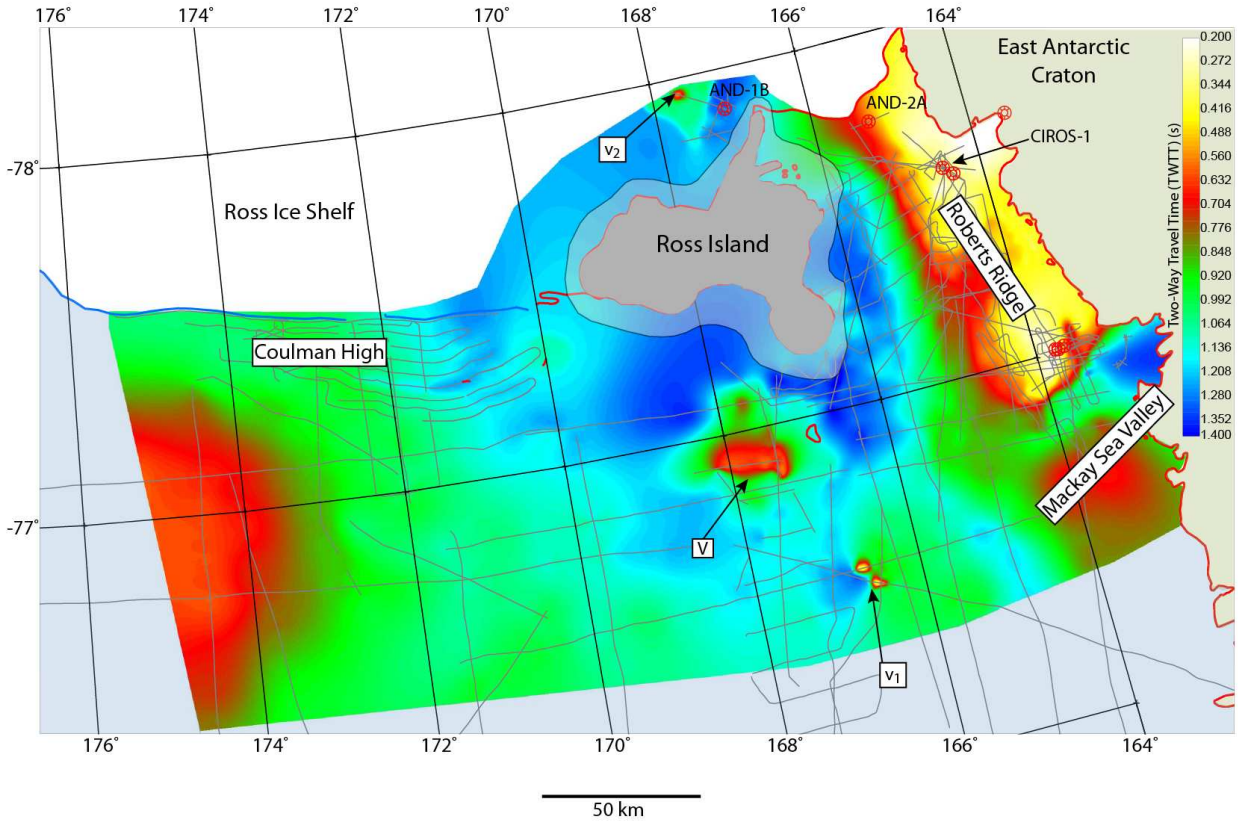

Figure 11. Time structure map of horizon RIB-r. This horizon represents the first depositional event following filling of the flexural basin surrounding Ross Island. The light gray outline surrounding Ross Island represents the edge of the Ross Island volcanic pile. Letters indicate features discussed in the text (V = volcanically disrupted area).

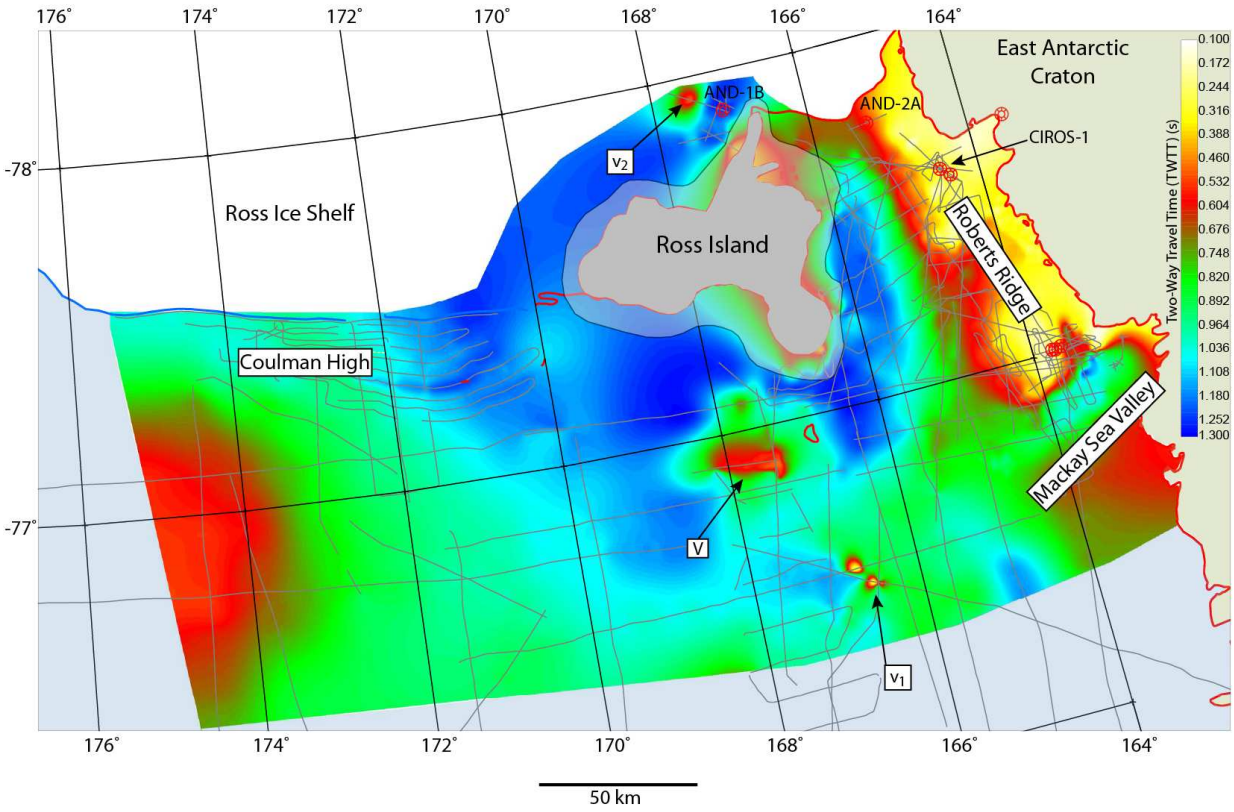

Figure 12. Time structure map of the modern seafloor. Letters indicate features discussed in the text (V, v_1, v_2 = volcanically disrupted areas).

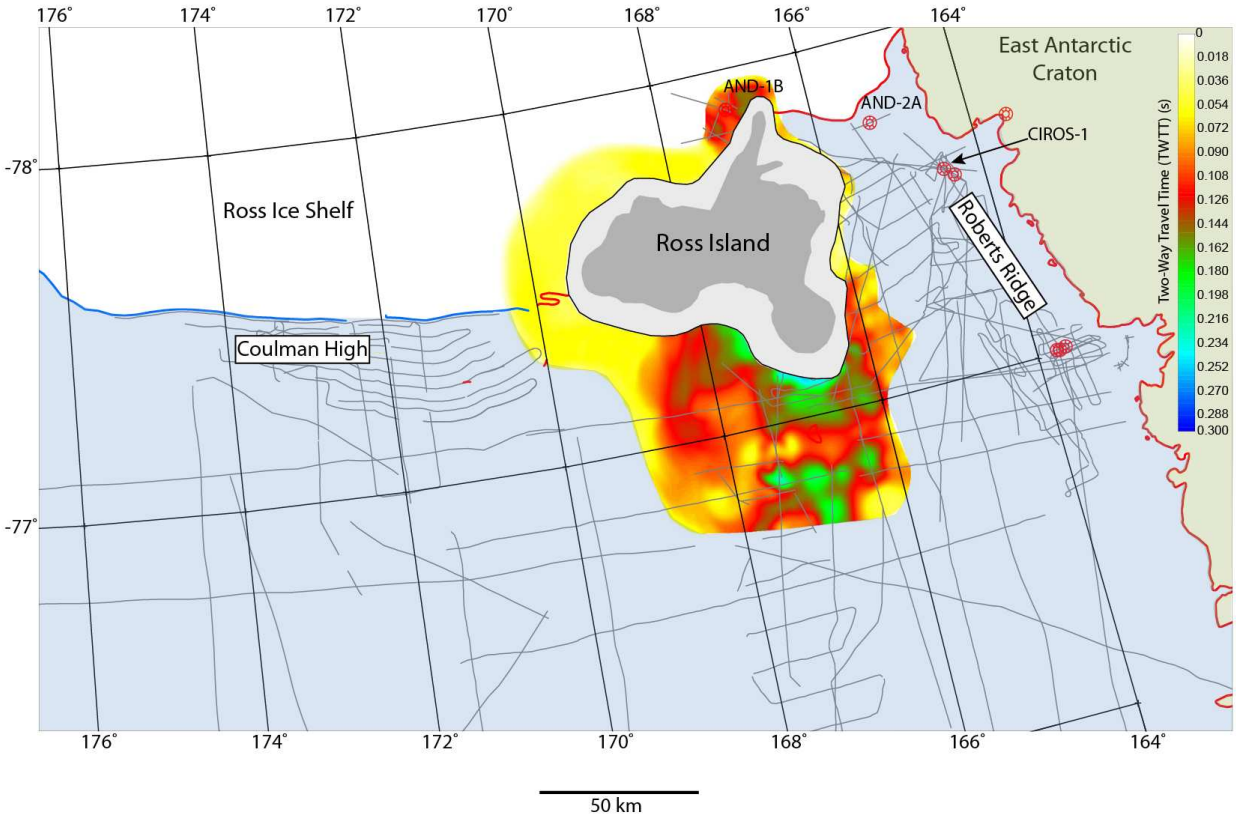

Figure 13. Isochron map of the RIM-g/RIM-b interval. The strata thickness shows the main N-S VLB trend, with the emergent Ross Island flexural moat superimposed. The light gray outline surrounding Ross Island represents the edge of the Ross Island volcanic pile.

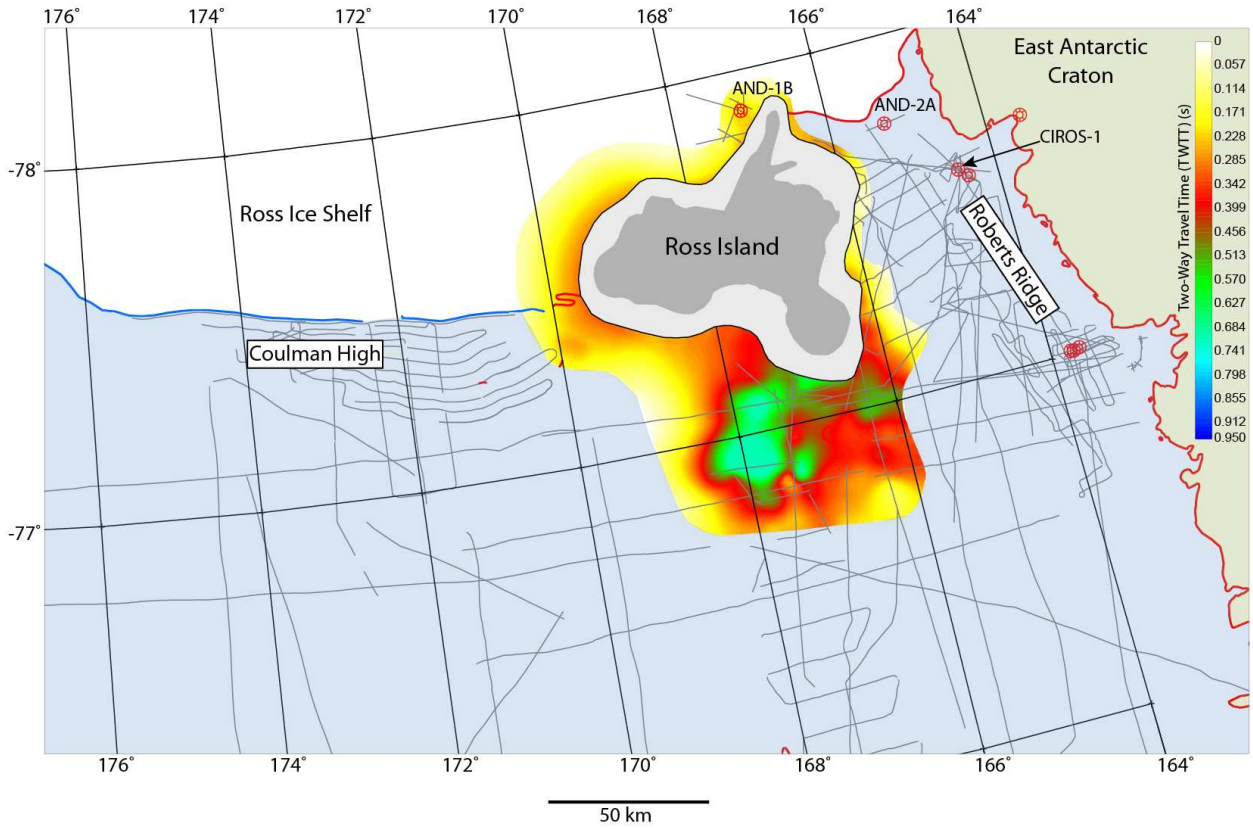

Figure 14. Isochron map of the RIM-b/RIB-r interval. The strata show an enclosing flexural moat around Ross Island, with the thickest strata north of the island. The light gray outline surrounding Ross Island represents the edge of the Ross Island volcanic pile.

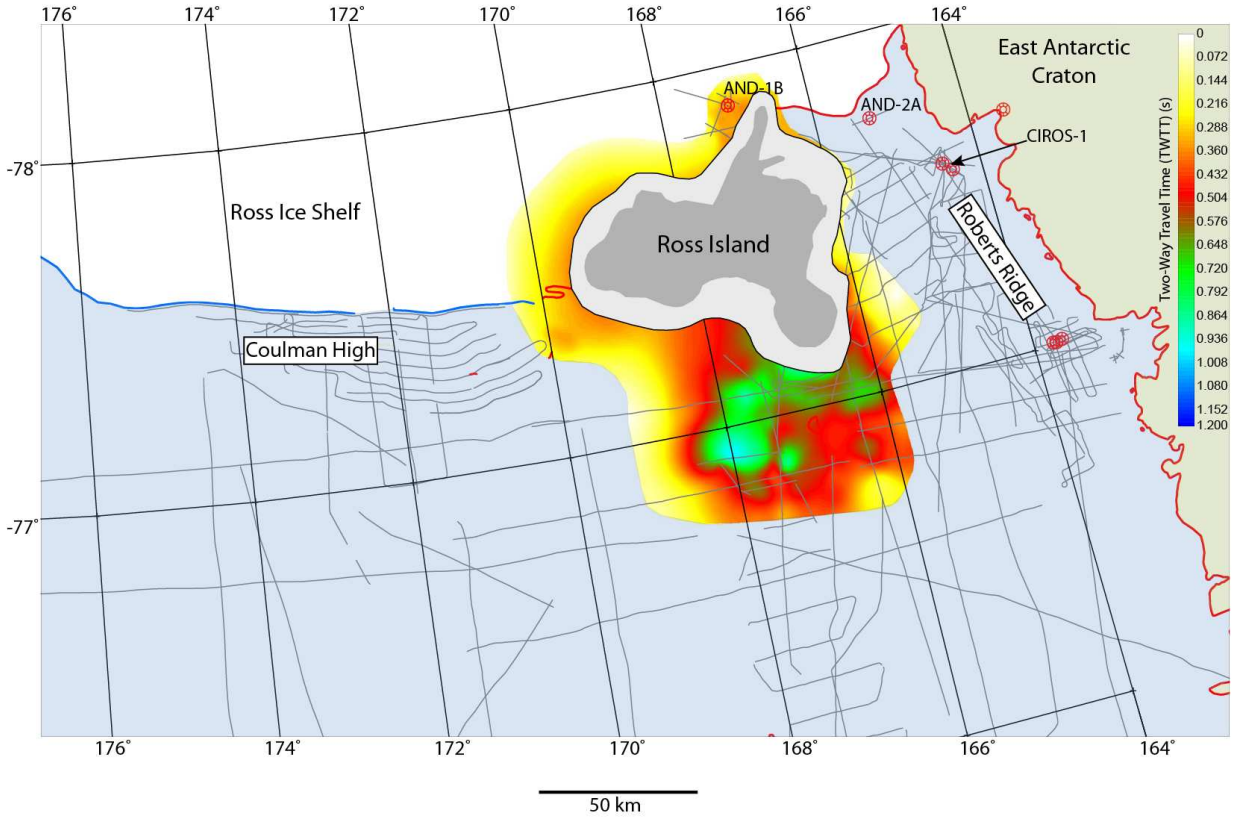

Figure 15. Isochron map of the RIM-g/RIB-r interval. The strata represent the total thickness of flexural strata around Ross Island. There is a clear enclosing moat, with the deepest portion located north of the island. The light gray outline surrounding Ross Island represents the edge of the Ross Island volcanic pile.

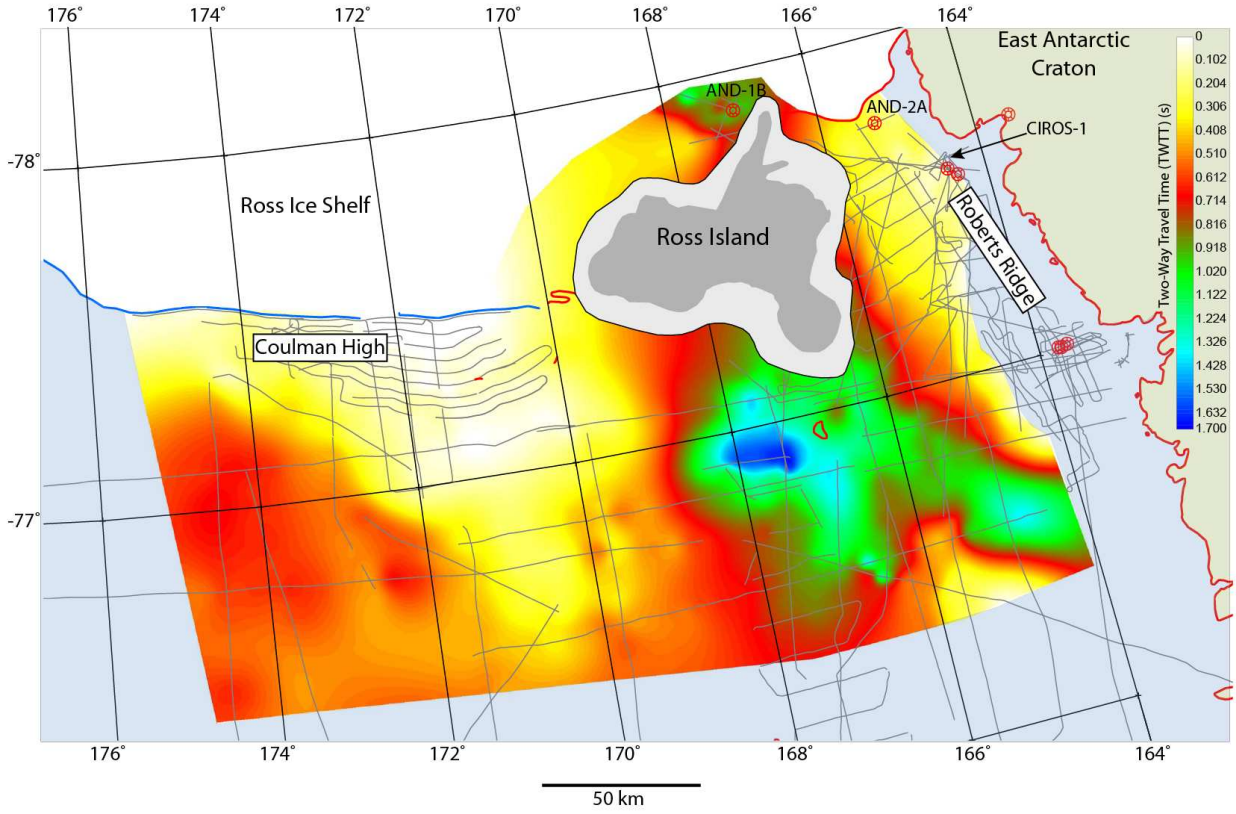

Figure 16. Isochron map of the RIB-m/RIB-r interval. The strata thickness shows the main N-S VLB trend and NNW trending VLB sub-basin. The light gray outline surrounding Ross Island represents the edge of the Ross Island volcanic pile.

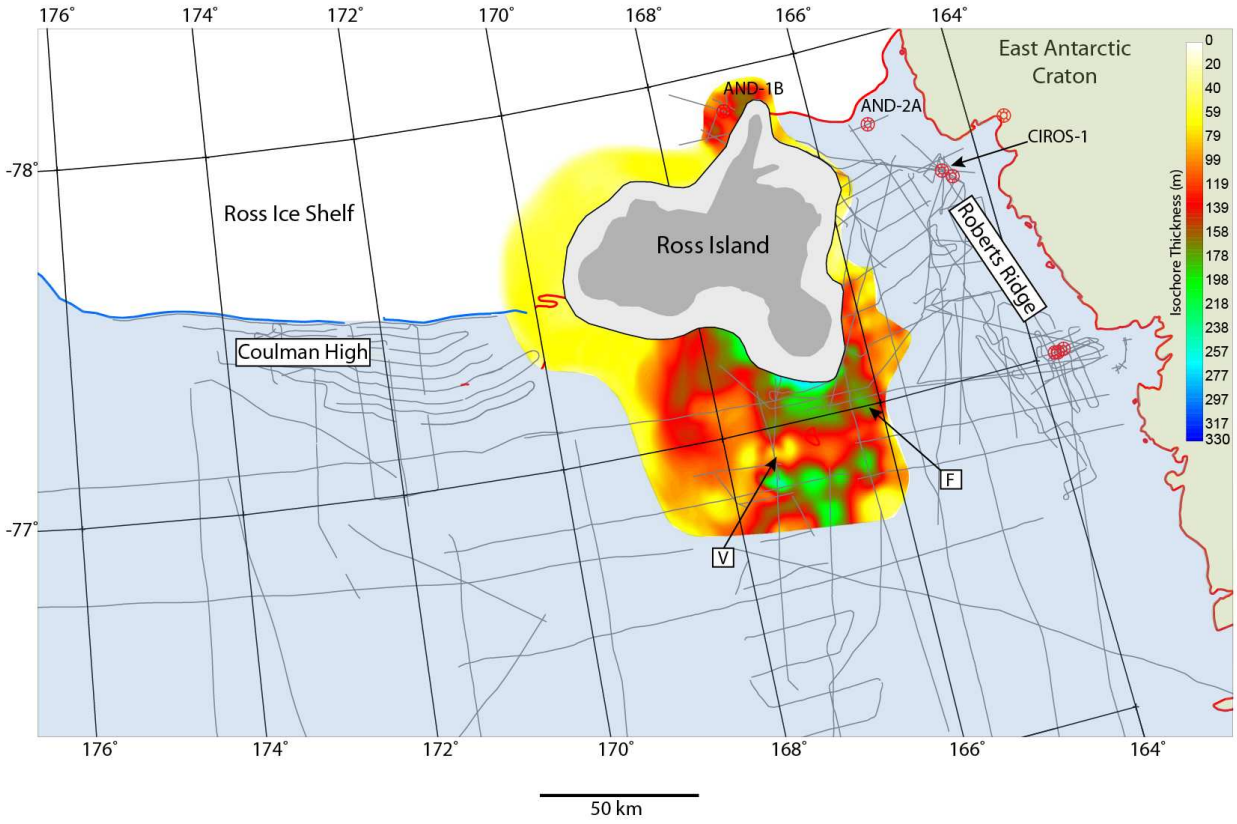

Figure 17. Isochore map of the RIM-g/RIM-b interval. Isochore thickness determined from Figure 13 using a constant interval velocity of 2178 m/s. Letters indicate features discussed in the text (V = volcanically disrupted area, F = fault-disrupted area). The light gray outline surrounding Ross Island represents the edge of the Ross Island volcanic pile.

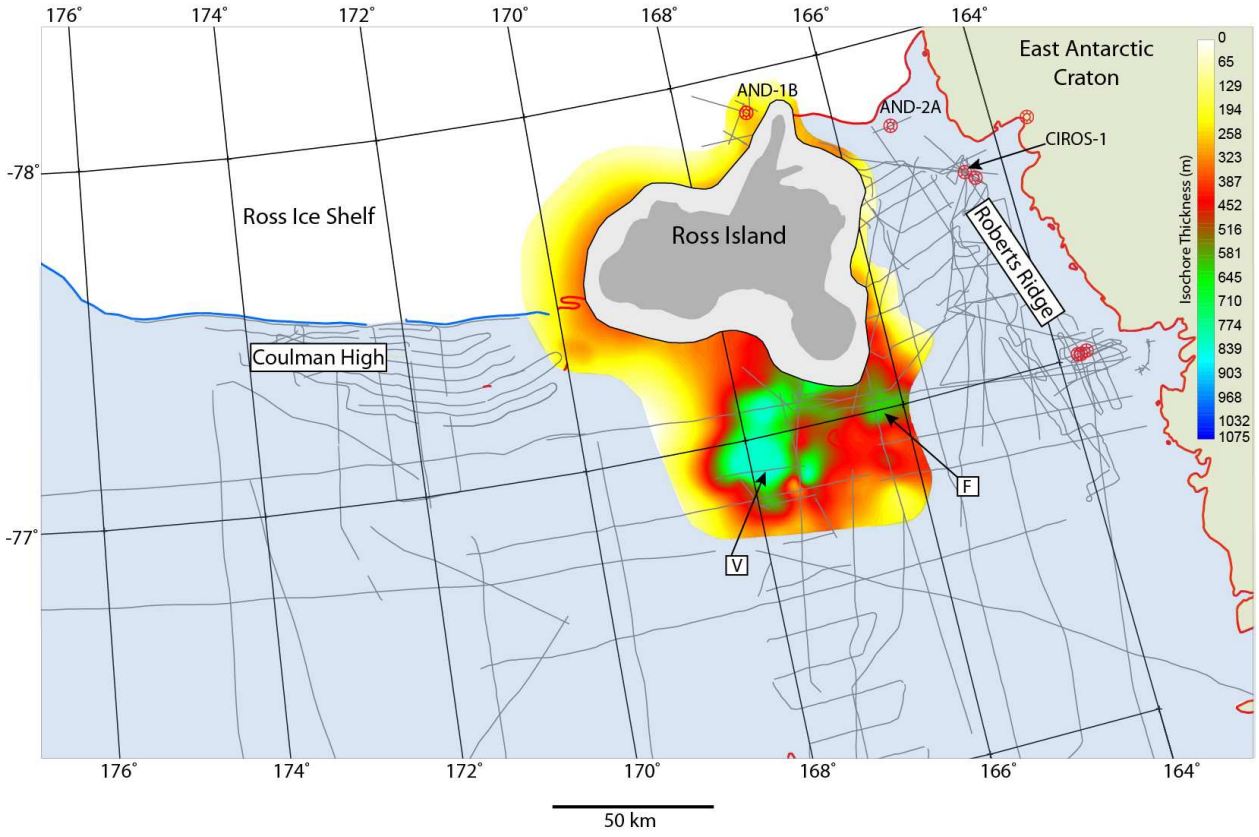

Figure 18. Isochore map of the RIM-b/RIB-r interval. Isochore thickness determined from Figure 14 using a constant interval velocity of 2328 m/s. Letters indicate features discussed in the text (V = volcanically disrupted area, F = fault-disrupted area). The light gray outline surrounding Ross Island represents the edge of the Ross Island volcanic pile.

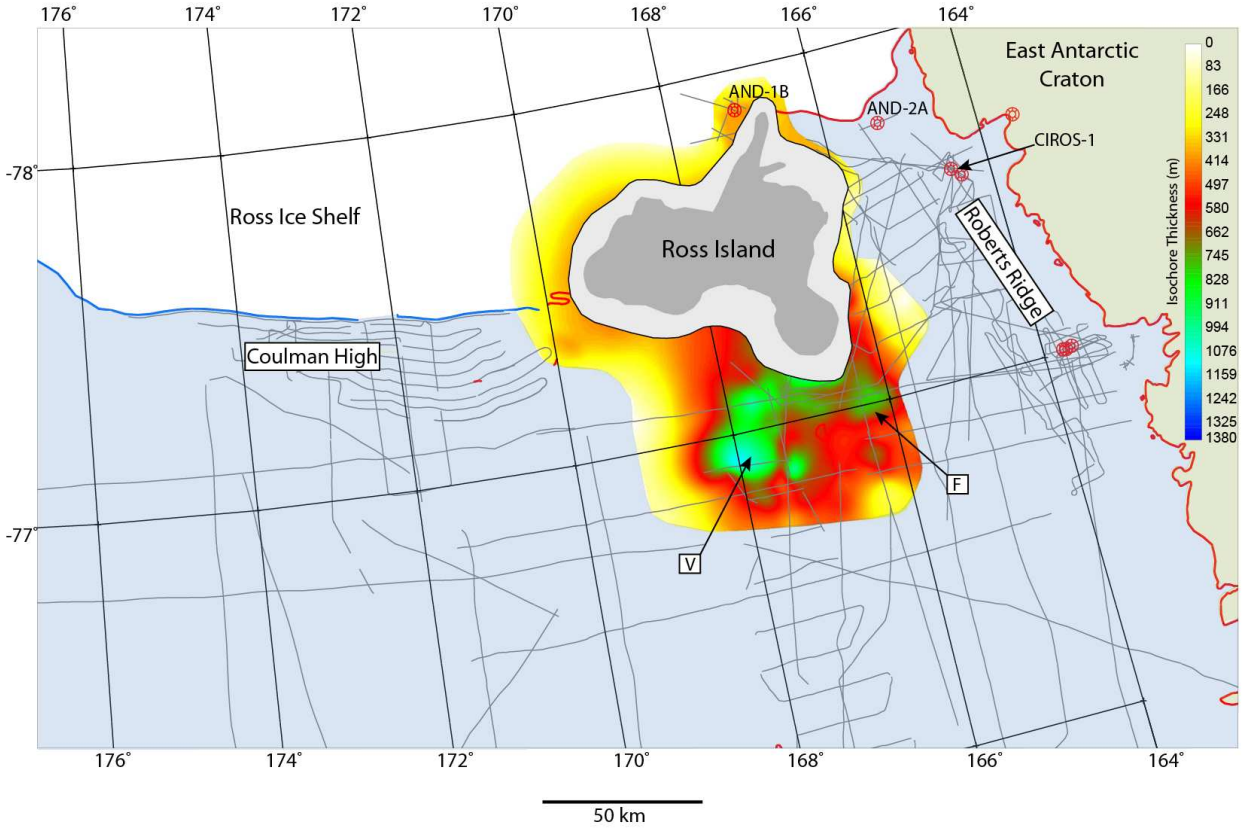

Figure 19. Isochore map of the RIM-g/RIB-r interval. Isochore thickness determined from Figure 15 using a constant interval velocity of 2281 m/s. Letters indicate features discussed in the text (V = volcanically disrupted area, F = fault-disrupted area). The light gray outline surrounding Ross Island represents the edge of the Ross Island volcanic pile.

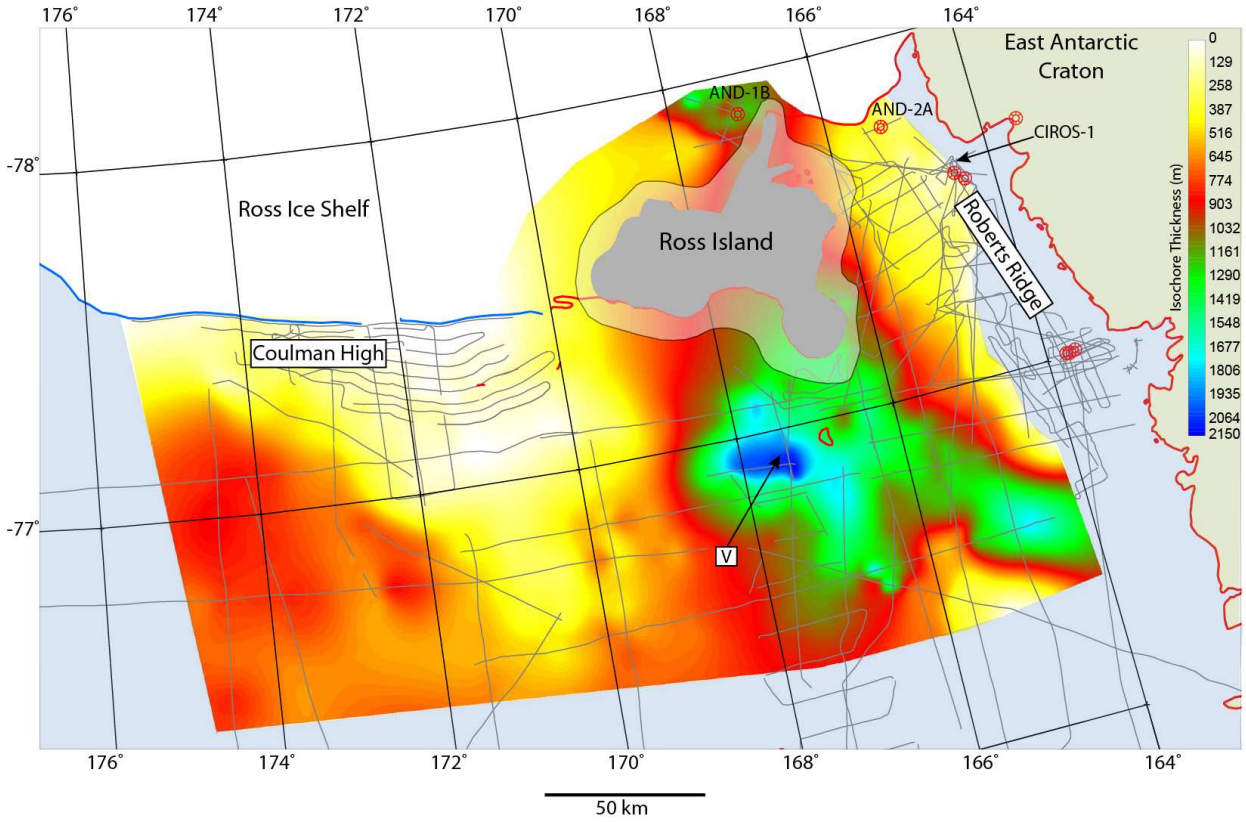

Figure 20. Isochore map of the RIB-m/RIB-r interval. Isochore thickness determined from Figure 16 using a constant interval velocity of 2535 m/s. Letters indicate features discussed in the text (V = volcanically disrupted area, F = fault-disrupted area). The light gray outline surrounding Ross Island represents the edge of the Ross Island volcanic pile.

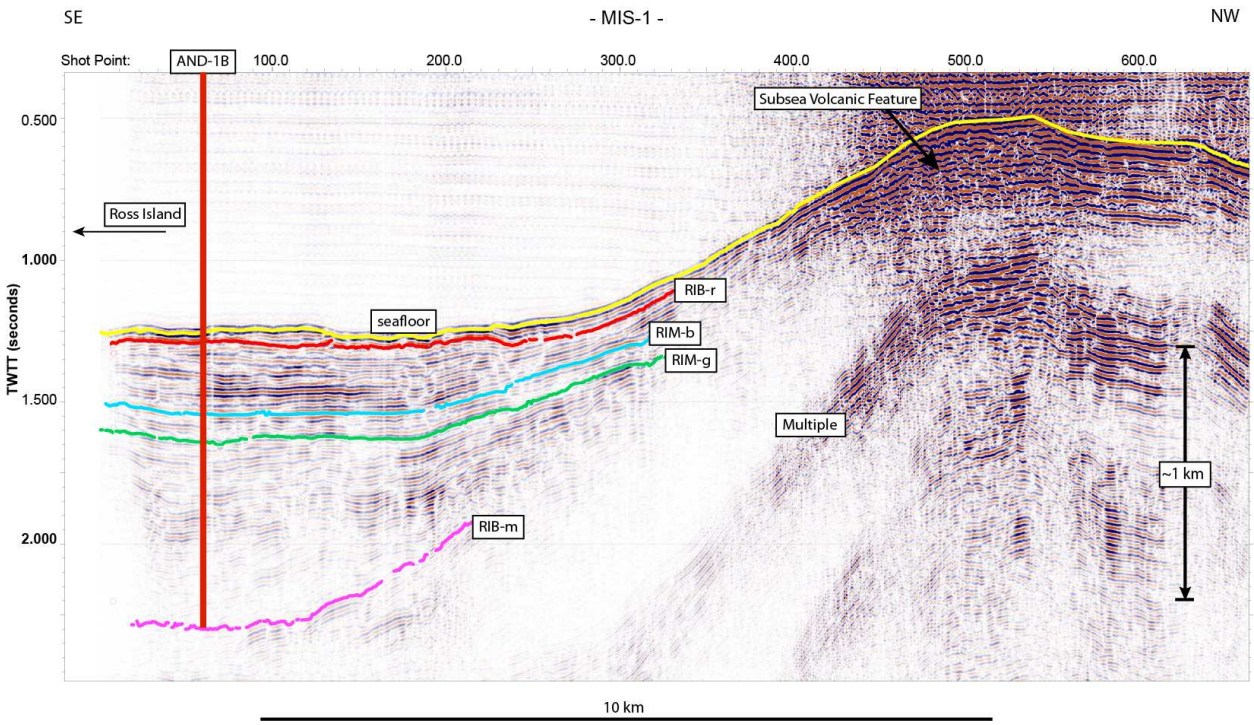

Figure 21. Seismic dip line MIS-1 on the southeast side of Ross Island that has been affected by flexure above horizon RIM-g (green).

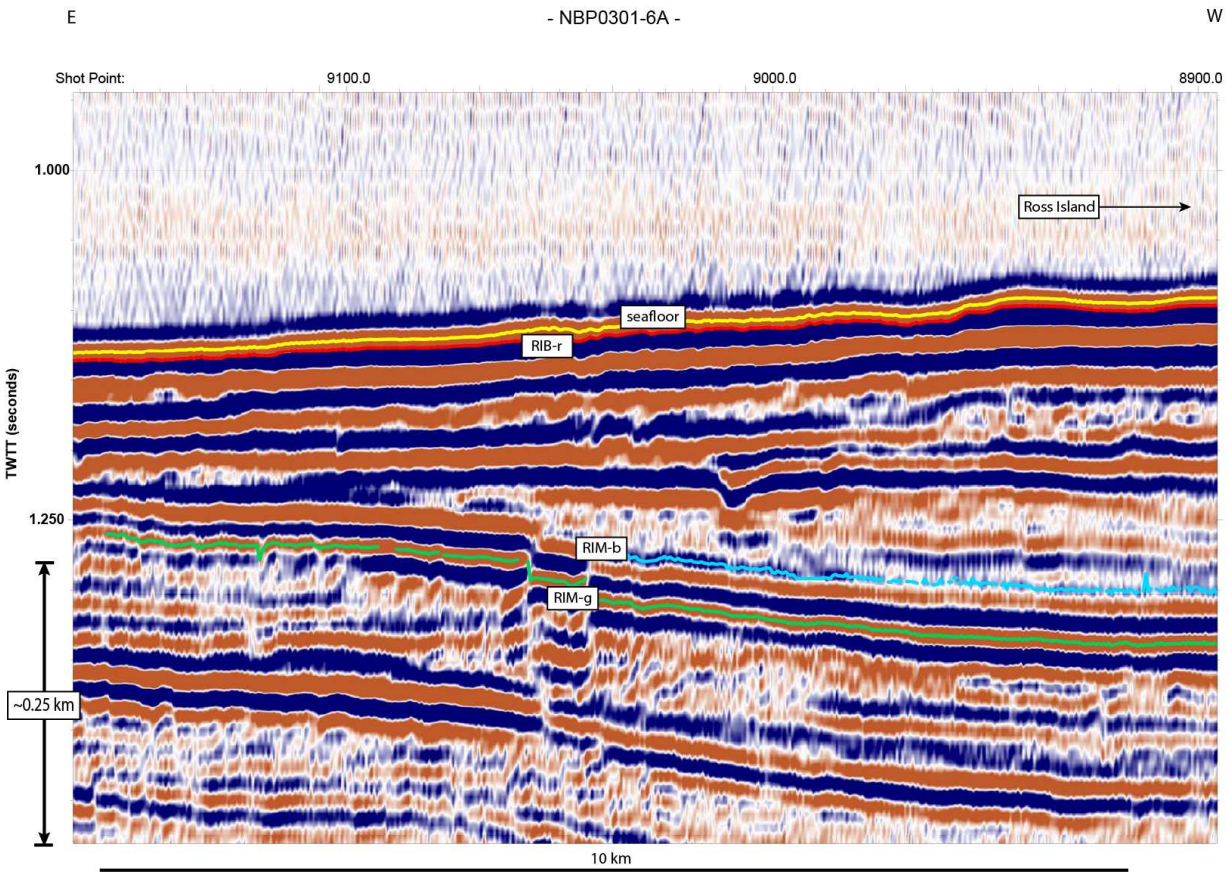

Figure 22. Western-most portion of seismic dip line NBP0301-6A on the east side of Ross Island that captures the edge of the flexural basin.

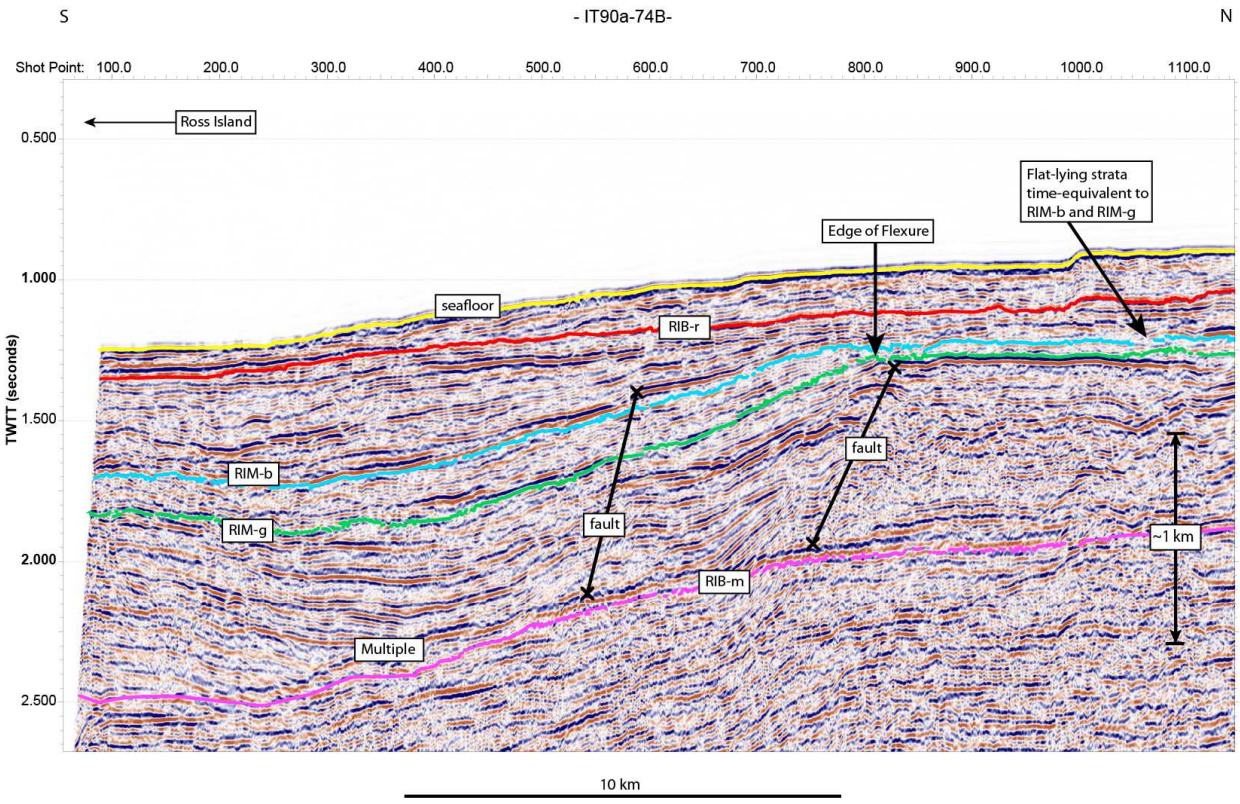

Figure 23. Southern-most portion of seismic strike line IT90a-74B. This seismic line captures the north edge of the flexural basin.

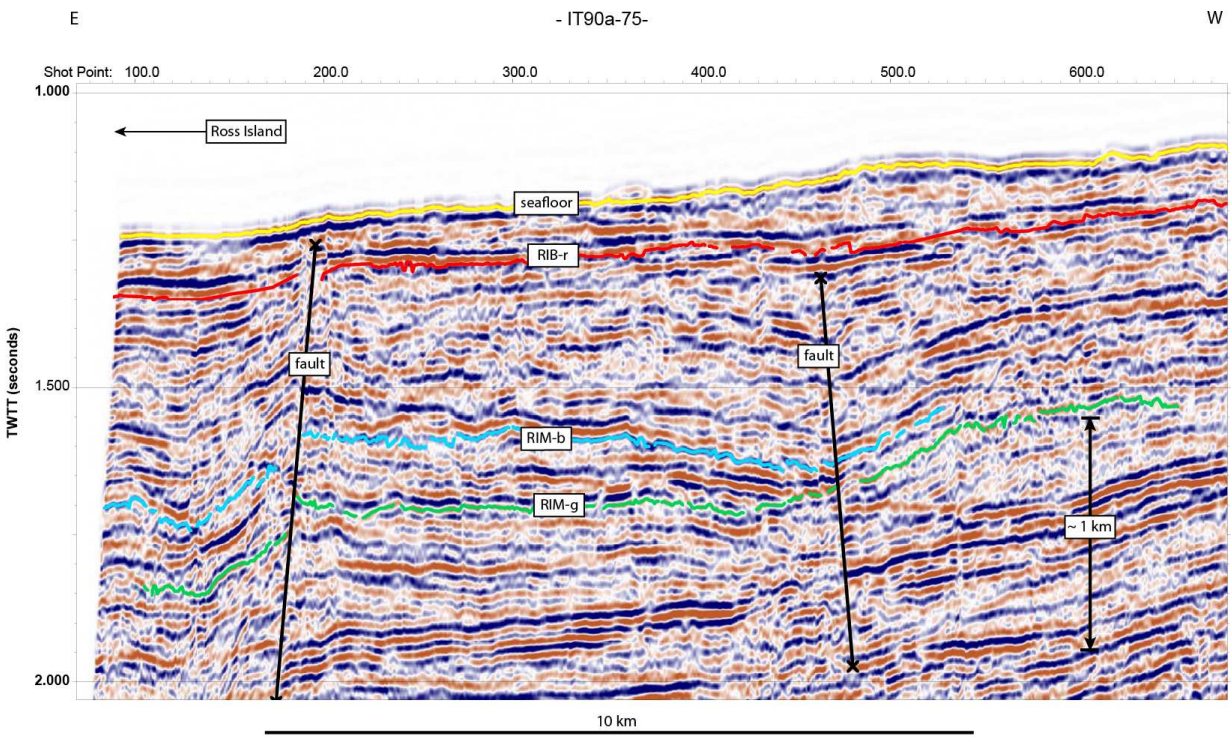

Figure 24. Eastern-most portion of seismic dip line IT90a-75. This seismic line captures an area of young faulting (nearly reaching the seafloor) that disrupt the flexural strata and cause horizons RIM-g and RIM-b to onlap deep in the stratigraphy.

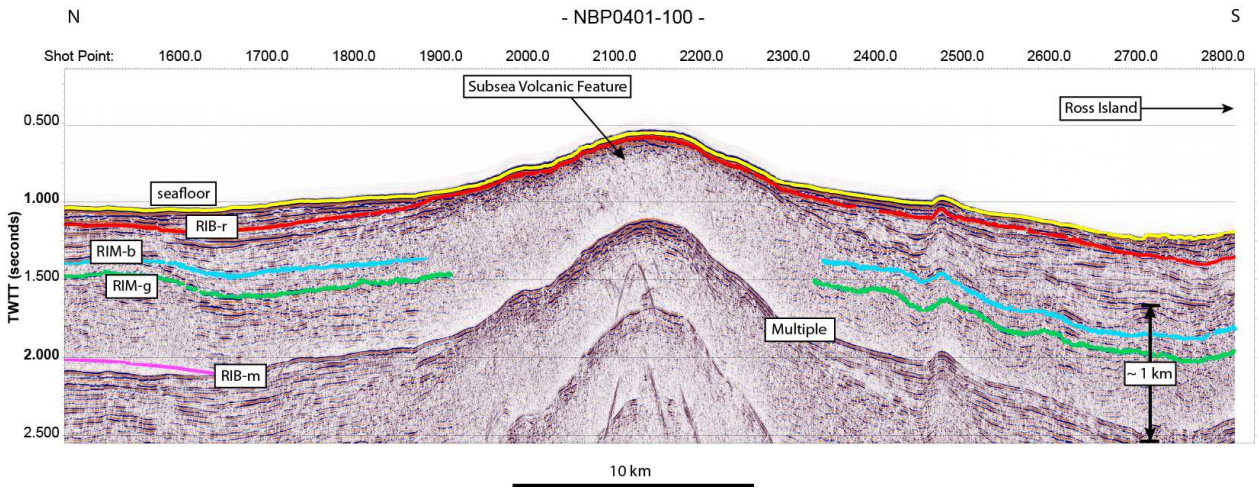

Figure 25. A portion of seismic strike line NBP0401-100 that captures a major volcanic feature disrupting the flexural strata north of Ross Island.

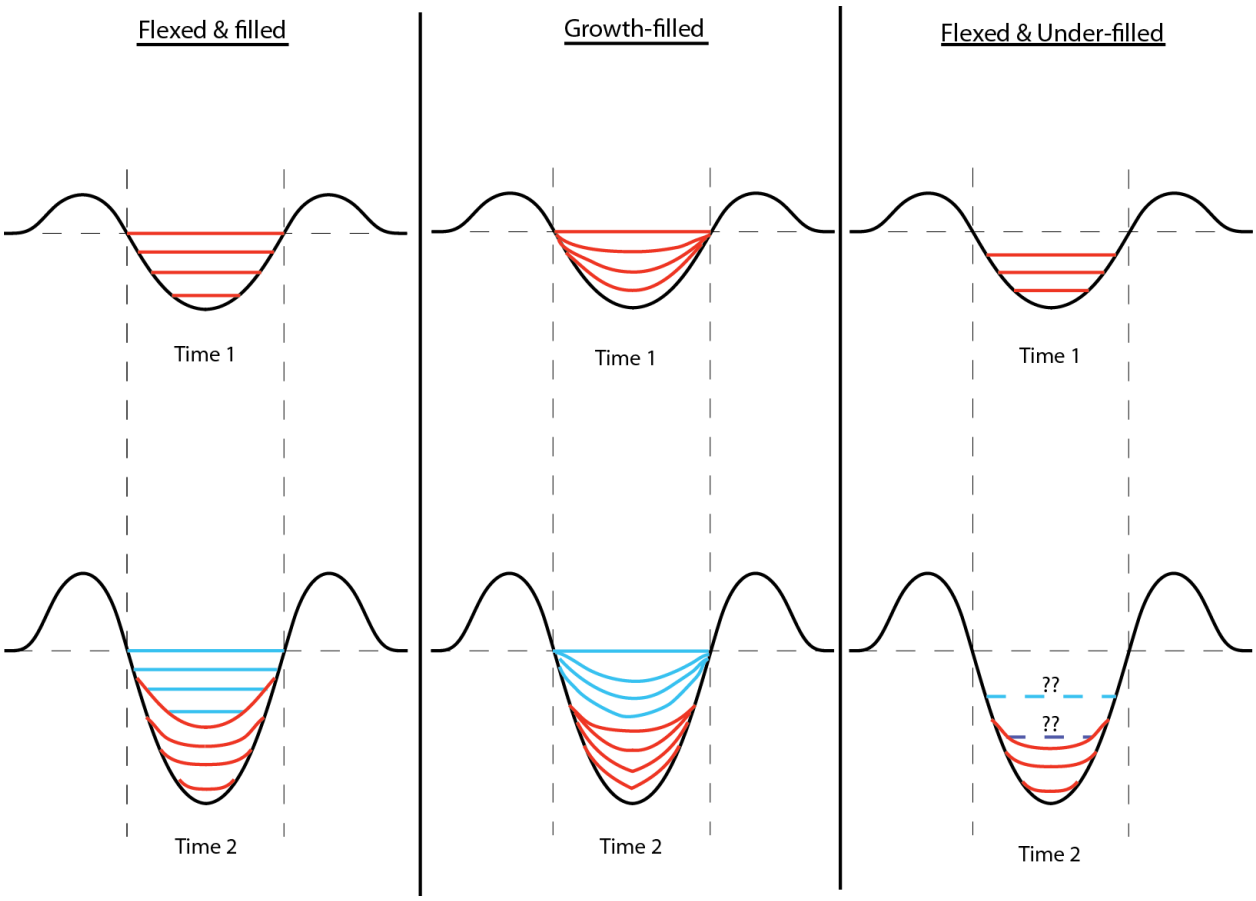

Figure 26. Schematic cartoon illustrating three flexural basin growth and filling models. "Time 1" represents the filled basin following the first flexural event. "Time 2" represents the filled basin following the second flexural event. Horizontal dashed line represents the original surface before flexure. Vertical dashed lines show the inflection point where the original surface is up-warped outside of the lines and down-warped inside of the lines. The flexed and filled model is explained by distinct flexural subsidence, followed by complete filling of the basin. Within the flexural packages, the onlap surface moves away from the basin, but individual depositional layers are parallel. The growth-filled model represents deposition as the basin subsides. Individual depositional layers thicken basin-ward. The flexed and under-filled model represents distinct flexural subsidence followed by under-filling of the basin. Subsequent flexure occurs, but the level of basin fill is limited by the sediment supply. The position of the distal pinchout of the sediment fill in the under-filled basin model will fluctuate depending on sediment supply and the amount of flexural subsidence

Age	Cooper et al., 1987	Brancolini et al., 1995	Bartek et al., 1996	Anderson and Bartek, 1992	Horgan et al., 2005	Fielding et al., 2008	This Paper
~7.6 Ma to Recent Upper Miocene to Recent	V1		A-B		Surface A0	Rk	RIB-r
		RSU 1?	C-D?	3/2?	Surface A1	Rj	RIM-b
			A-H				RIM-g
		RSU 2	E-F	5/6	Surface A2	Ri	
		RSS 5-8 RSU 4 RSS 4	G-H				
~13 -~7.6 Ma Middle Miocene to Upper Miocene		RSU 4a		9/10	Surface B	Rh	
	V2	RSS 3					
23-~13 ma Lower to Middle Miocene		RSU 5	L-M	10/11	Surface C	Rg	RIB-m
	V3	RSS 2					
		~RSU 6	P/Q			Rf	
		RSS 1					
			R/S				
	V4						
29-23 Ma Lower to Upper Oligocene			T			Re	
	V5						
						Rd	
						Rc	
34-29 Ma Eocene to Lower Oligocene						Rb	
						Ra	
	V6		("volcanics")				
	V7		("basement")				

Table 1. Seismic stratigraphic framework for the western Ross Sea with horizons from this study added (modified from Fielding et al., 2008).

CHAPTER 3 - RECOMMENDATIONS FOR FUTURE WORK

The evolution of the flexural basin surrounding Ross Island has been well detailed by this study. However, many questions remain unanswered. Flexural modeling of the Ross Island moat will be important to determine the strength of the lithosphere underlying the region through time. Mapping the structures more thoroughly should also be completed. It appears that two fault populations exist, a young population that cuts to the seafloor and an older population that lies below much of the flexural moat strata. The northern shifted depocenter of the Ross Island flexural basin suggests additional structure mapping should be completed in that area in order to determine the total effect of faulting on the flexural stratigraphy. Emergence of the Terror Rift within the Victoria Land Basin could be the cause of the youngest population of faults that cut to the seafloor, and would be young enough to affect the flexural strata. The fault-bounded nature of the stratigraphic highs flanking Ross Island (Coulman High and Roberts Ridge) is obvious from stratigraphic mapping. Fault mapping on the edge of these highs could provide additional insight into the formation of the Victoria Land Basin, especially around the time that horizon RIB-m was deposited (ca. 13 Ma).

The pink erosional surface seen on seismic line NBP0401-126m (Fig. 6A, 6B) deserves additional study as well. It provides strong evidence for glacial scouring between ca. 13 Ma (horizon RIB-m) and ca. 4 Ma (horizon RIM-g). Mapping of this horizon could provide insight to the extent of glacial scouring below the Ross Island flexural basin, and ideally would be correlated back to the boreholes to estimate an age of the scoured surface. The strata lying between this scour surface and horizon RIM-g on seismic line NBP0401-126m appear to be flexural in nature. Onlapping occurs progressively up-dip, just as the flexural wedges show

between RIM-g/RIM-b and RIM-b/RIB-r. Mapping of the strata that onlap the scoured horizon could provide insight to the extent of the scouring, and the effect (if any) that the scouring had on creating accommodation space just prior to flexural subsidence and basin filling by horizon RIM-g.

The age of magmatism north of the island in relation to the flexural strata has proven to be a challenge based on seismic stratigraphic mapping alone. The conclusion reached here is that horizon RIB-m represents a surface that volcanic eruptions built upon sometime after deposition of the horizon ca. 13 Ma. Flexural strata are uplifted and disturbed by the volcanics north of the island, implying that volcanism post-dated the flexural strata as well. Subsequent volcanic eruptions then thickened the strata overlying horizon RIM-b, artificially thickening the youngest flexural sequence north of the island. This hypothesis could benefit from detailed study, as other interpretations of magmatic timing are possible (i.e. the magmatism post-dates RIB-m as well, and thus is older than 13 Ma which would change the time-structure and isochore maps involving that horizon).

The results suggest that the AND-1B borehole was drilled into a thinner, narrower portion of the flexural moat south of Ross Island. Additional drilling efforts could prove useful if focused on the flexural moat on the north side of the island, where our isochore maps indicate the moat is deepest. It would be useful to add another data point to compare with the AND-1B core. Differences in lithology, depositional processes, presence (or lack of) volcanic layers, true thickness of the Plio-Pleistocene section, and age dates of the strata would provide a much needed constraint on the flexural moat stratigraphy. Additional seismic data on the east and southeast sides of the island would also be useful to more accurately determine the spatial extent and thickness of moat-fill strata mapped by our study. Wide-azimuth refraction surveys may also

be useful in unraveling the complex interplay between magmatic edifice building events and sedimentary deposition of strata into the flexural moat.

REFERENCES

Acton, G., Crampton, J., Di Vincenzo, G., Fielding, Christopher R., Florindo, F., Hannah, M., Harwood, D. M., Ishman, S., Johnson, K., Jovane, L., Levy, R., Lum, B., Marcano, M. C., Mukasa, S., Ohneiser, C., Olney, M. P., Riesselman, C., Sagnotti, L., Stefano, C., Strada, E., Taviani, M., Tuzzi, E., Verosub, K. L., Wilson, G. S., Zattin, M., and the ANDRILL-SMS Science Team, 2008, Preliminary Integrated Chronostratigraphy of the AND-2A Core, ANDRILL, Southern McMurdo Sound Project, Antarctica: Terra Antarctica, v. 15, no. 1, p. 211-220.

Aitken, A.R.A., Wilson, G.S., Jordan, T., Tinto, K., and Blakemore, H., 2012, Flexural controls on late Neogene basin evolution in southern McMurdo Sound, Antarctica: Global and Planetary Change, v. 80-81, no. January 2012, p. 99-112, doi: 10.1016/j.gloplacha.2012.02.004.

Anderson, J.B., and Bartek, L.R., 1992, Cenozoic glacial history of the Ross Sea revealed by intermediate resolution seismic reflection data combined with drill site information, *in* Kennett, J.P., and Warnke, D.A., eds., The Antarctic Paleoenvironment: A Perspective on Global Change, Part 1, Antarctic Research Series, v. 56, American Geophysical Union, Washington, D.C., p. 231-263.

Armstrong, R.L., 1978, K-Ar dating: Late Cenozoic McMurdo Volcanic Group and dry valley glacial history, Victoria Land, Antarctica: New Zealand Journal of Geology and Geophysics, v. 21, no. 6, p. 685-698, doi: 10.1080/00288306.1978.10425199.

Barrett, P.J., and McKelvey, B.C., 1981, Cenozoic glacial and tectonic history of the Transantarctic Mountains in the McMurdo Sound region: recent progress from drilling and related studies: Polar Record, v. 20, no. 129, p. 543-548.

Barrett, P.J., Elston, D.P., Harwood, D.M., McKelvey, B.C., and Webb, P.-N., 1987, Mid-Cenozoic record of glaciation and sea-level change on the margin of the Victoria Land basin, Antarctica: Geology, v. 15, no. 7, p. 634-637.

Barrett, P.J., Hambrey, M.J., and Robinson, P.R., 1991, Cenozoic glacial and tectonic history from CIROS-1, McMurdo Sound, *in* Thomson, M.R.A., Crame, J.A., and Thomson, J.W., eds., Geological Evolution of Antarctica: Cambridge University Press, New York, pp. 651-656.

Barrett, P.J., Henrys, S.A., Bartek, L.R., Brancolini, G., Busetti, M., Davey, F.J., Hannah, M.J., and Pyne, A.R., 1995, Geology of the margin of the Victoria Land Basin off Cape Roberts, southwest Ross Sea, *in* Cooper, A.K., Barker, P.F., and Brancolini, G., eds., Geology and Seismic Stratigraphy of the Antarctic Margin: Antarctic Research Series, v. 68, American Geophysical Union, Washington, D.C., p. 183-207.

Bartek, L.R., Vail, P.R., Anderson, J.B., Emmet, P.A., and Wu, S., 1991, Effect of Cenozoic Ice Sheet Fluctuations in Antarctica on the Stratigraphic Signature of the Neogene: Journal of Geophysical Research, v. 96, no. B4, p. 6753-6778.

Bartek, L.R., Henrys, S.A., Anderson, J.B., and Barrett, P.J., 1996, Seismic stratigraphy of McMurdo Sound, Antarctica: implications for glacially influenced early Cenozoic eustatic change?: Marine Geology, v. 130, no. 1-2, p. 79-98.

Behrendt, J.C., LeMasurier, W.E., Cooper, A.K., Tessensohn, F., Tréhu, A., and Damaske, D., 1991, Geophysical Studies of the West Antarctic Rift System: Tectonics, v. 10, no. 6, p. 1257-1273.

Behrendt, J.C., Blankenship, D.D., Finn, C.A., Bell, R.E., Sweeney, R.E., Hodge, S.M., and Brozena, J.M., 1994, CASERTZ aeromagnetic data reveal late Cenozoic flood basalts(?) in the West Antarctic rift system: Geology, v. 22, no. 6, p. 527-530.

Behrendt, J.C., Saltus, R., Damaske, D., McCafferty, A., Finn, C.A., Blankenship, D., and Bell, R.E., 1996, Patterns of late Cenozoic volcanic and tectonic activity in the West Antarctic rift system revealed by aeromagnetic surveys: Tectonics, v. 15, no. 2, p. 660-676.

Behrendt, J.C., 1999, Crustal and lithospheric structure of the West Antarctic Rift System from geophysical investigations – a review: Global and Planetary Change, v. 23, no. 1-4, p. 25-44.

Betterly, S.J., Speece, M.A., Levy, R.H., Harwood, D.M., and Henrys, S.A., 2007, A Novel Over-Sea-Ice Seismic Reflection Survey in McMurdo Sound, Antarctica: Terra Antarctica, v. 14, no. 2, p. 97-106.

Brancolini, G., Cooper, A.K., and Coren, F., 1995, Seismic facies and glacial history in the Western Ross Sea (Antarctica), *in* Cooper, A.K., Barker, P.F., and Brancolini, G., eds., Geology and Seismic Stratigraphy of the Antarctic Margin: Antarctic Research Series, v. 68, American Geophysical Union, Washington, D.C., p. 209-233.

Briggs, I.C., 1974, Machine Contouring Using Minimum Curvature: Geophysics, v. 29, no. 1, doi: 10.1190/1.1440410.

Bucker, C.J., 1998, Porosity and sound velocity measured in sediment core CIROS-1, doi: 10.1594/PANGAEA.54717, *supplement to* Bucker, C.J., Henrys, S., and Wonik, T., 1998, Revision of the Cenozoic seismic velocity structure of the CIROS-1 drillhole, Antarctica,

and implications for further drilling off Cape Roberts: Terra Antarctica, v. 5, no. 3, p. 281-289.

Cande, S.C., Stock, J.M., Müller, R.D., and Ishihara, T., 2000, Cenozoic motion between East and West Antarctica: Nature, v. 404, no. 6774, p. 145-150.

Cande, S.C., and Stock, J.M., 2006, Constraints on the Timing of Extension in the Northern Basin, Ross Sea, *in* Futterer, D.K., Damaske, D., Kleinschmidt, G., Miller, H., and Tessensohn, F., eds., Antarctica: Contributions to Global Earth Science, Springer, New York, p. 319-326.

Cape Roberts Science Team, 2000, Studies from the Cape Roberts Project, Ross Sea, Antarctica: Summary of Results: Initial Report on CRP-3: Terra Antarctica, v. 7, no. 1/2, p. 185-203.

Cooper, A.K., Davey, F.J., and Behrendt, J.C., 1987, Seismic Stratigraphy and Structure of the Victoria Land Basin, Western Ross Sea, Antarctica, *in* Cooper, A.K., and Davey, F.J., eds., The Antarctica Continental Margin: Geology and Geophysics of the Western Ross Sea, CPCEMR Earth Science Series:, v. 5B: Houston, Texas, Circum-Pacific Council for Energy and Mineral Resources, p. 27-76.

Cooper, A.K., Davey, F.J., and Hinz, K., 1991, Crustal extension and origin of sedimentary basins beneath the Ross Sea and Ross Ice Shelf, Antarctica, *in* Thomson, M.R.A., Crame, J.A., and Thomson, J.W., eds., Geological Evolution of Antarctica: Cambridge University Press, New York, pp. 285-292.

Davey, F.J., and Christoffel, D.A., 1984, The correlation of MSSTS-1 drillhole results with seismic reflection data from McMurdo Sound, Antarctica: New Zealand Journal of Geology and Geophysics, v. 24, no. 4, p. 405-412, doi: 10.1080/00288306.1984.10422262.

Davey, F.J., and Cooper, A.K., 1987, Gravity studies of the Victoria Land basin and Iselin Bank, *in* Cooper, A.K., and Davey, F.J., eds., The Antarctica Continental Margin: Geology and Geophysics of the Western Ross Sea, CPCEMR Earth Science Series:, v. 5B: Houston, Texas, Circum-Pacific Council for Energy and Mineral Resources, p. 119-138.

Davey, F.J., and Brancolini, G., 1995, The Late Mesozoic and Cenozoic Structural Setting of the Ross Sea Region, *in* Cooper, A.K., Barker, P.F., and Brancolini, G., eds., Geology and Seismic Stratigraphy of the Antarctic Margin: Antarctic Research Series, v. 68, American Geophysical Union, Washington, D.C., p. 167-182.

Davey, F.J., Brancolini, G., Hamilton, R.J., Henrys, S.A., Sorlien, C.C., and Bartek, L.R., 2000, A Revised Correlation of the Seismic Stratigraphy at the Cape Roberts Drill Sites with the Seismic Stratigraphy of the Victoria Land Basin, Antarctica: Terra Antarctica, v. 7, no. 3, p. 215-220.

Davey, F.J., Barrett, P.J., Cita, M.B., van der Meer, J.J.M., Tessensohn, F., Thomson, M.R.A., Webb, P.-N., and Woolfe, K.J., 2001, Drilling for Antarctic Cenozoic climate and tectonic history at Cape Roberts, southwestern Ross Sea: EOS Transactions, v. 82, no. 48, p. 585-590. Doi: 10.1029/01EO00339.

Davey, F.J., Cande, S.C., and Stock, J.M., 2006, Extension in the western Ross Sea region – links between Adare Basin and Victoria Land Basin: Geophysical Research Letters, v. 33, no. 20, L20315, doi: 10.1029/2006GL027383.

Decesari, R.C., Wilson, D.S., Luyendyk, B.P., and Faulkner, M., 2007, Cretaceous and Tertiary extension throughout the Ross Sea, Antarctica: U.S. Geological Survey and The National Academies Open-file Report 2007-1047, Short Research Paper 098, doi: 10.3133/of2007-1047.srp098.

De Santis, L., Davey, F.J., Prato, S., and Brancolini, G., 2001, Subsidence at the Cape Roberts (CRP) Drillsites from Backstripping Techniques, Victoria Land Basin, Antarctica: Terra Antarctica, v. 8, no. 3, p. 137-141.

Dunbar, G.B., 2009, Physical properties of sediment core AND-2A, doi: 10.1594/PANGAEA.744014, *supplement to* Dunbar, G.B., Atkins, C., Magens, D., Niessen, F., and the SMS Science Team, 2009, Physical Properties of the AND-2A Core, ANDRILL Southern McMurdo Sound Project, Antarctica: Terra Antarctica, v. 15, no. 1, p. 49-56.

Eagles, G., 2003, Tectonic evolution of the Antarctic-Phoenix plate system since 15 Ma: Earth and Planetary Science Letters, v. 217, no. 1-2, p. 97-109, doi: 10.1016/S0012-821X(03)00584-3.

Eagles, G., Gohl, K., and Larter, R.D., 2004, High-resolution animated tectonic reconstruction of the South Pacific and West Antarctic Margin: Geochemistry Geophysics Geosystems, v. 5, no. 7, Q07002, doi: 10.1029/2003GC000657.

Eagles, G., Gohl, K., and Larter, R.D., 2009, Animated tectonic reconstruction of the Southern Pacific and alkaline volcanism at its convergent margins since Eocene times: Tectonophysics, v. 464, no. 1-4, p. 21-29, doi: 10.1016/j.tecto.2007.10.005.

Esser, R.P., Kyle, P.R., and McIntosh, W.C., 2004, $^{40}Ar/^{39}Ar$ dating of the eruptive history of Mount Erebus, Antarctica: volcano evolution: Bulletin of Volcanology, v. 66, no. 8, p. 671-686.

Fielding, C.R., Woolfe, K.J., Howe, J.A., and Lavelle, M.A., 1998, Sequence stratigraphic analysis of CRP-1, Cape Roberts Project, McMurdo Sound, Antarctica: Terra Antarctica, v. 5, no. 3, p. 353-361.

Fielding, C.R., Naish, T.R., Woolfe, K.J., and Lavelle, M.A., 2000, Facies analysis and sequence stratigraphy of CRP-2/2A, Victoria Land Basin, Antarctica: Terra Antarctica, v. 7, no. 3, p. 323-338.

Fielding, C.R., Naish, T.R., and Woolfe, K.J., 2001, Facies architecture of the CRP-3 drillhole, Victoria Land Basin, Antarctica: Terra Antarctica, v. 8, no. 3, p. 217-224.

Fielding, C.R., Henrys, S.A., and Wilson, T.J., 2006, Rift History of the Western Victoria Land Basin: A new Perspective Based on Integration of Cores with Seismic Reflection Data, *in* Futterer, D.K., Damaske, D., Kleinschmidt, G., Miller, H., and Tessensohn, F., eds., Antarctica: Contributions to Global Earth Sciences, Springer-Verlag, Berlin, p. 309-318.

Fielding, C.R., Whittaker, J., Henrys, S.A., Wilson, T.J., and Naish, T.R., 2008, Seismic facies and stratigraphy of the Cenozoic succession in McMurdo Sound, Antarctica: Implications for tectonic, climatic, and glacial history: Palaeogeography, Palaeoclimatology, Palaeoecology, v. 260, no. 1-2, p. 8-29.

Fielding, C.R., Browne, G.H., Field, B., Florindo, F., Harwood, D.M., Krissek, L.A., Levy, R.H., Panter, K.S., Passchier, S., and Pekar, S.F., 2011, Sequence stratigraphy of the ANDRILL AND-2A drillcore, Antarctica: A long-term, ice-proximal record of Early to Mid-Miocene climate, sea-level and glacial dynamism: Palaeogeography, Palaeoclimatology, Palaeoecology, v. 305, no. 1-4, p. 337-351.

Fitzgerald, P.G., 1992, The Transtantarctic Mountains of southern Victoria Land: the application of apatite fission track analysis to a rift shoulder uplift: Tectonics, v. 11, no. 3, p. 634-662.

Florindo, F., Wilson, G.S., Roberts, A.P., Sagnotti, L., and Verosub, K.L., 2005, Magnetostratigraphic chronology of a late Eocene to early Miocene glacimarine succession

from the Victoria Land Basin, Ross Sea, Antarctica: Global and Planetary Change, v. 45, no. 1-3, p. 207-236, doi: 10.1016/j.gloplacha.2004.09.009.

Florindo, F., Harwood, D.M., Talarico, F., Levy, R.H., and the ANDRILL-SMS Science Team, 2008, Background to the ANDRILL Southern McMurdo Sound Project, Antartica: Terra Antarctica, v. 15, no. 1, p. 13-20.

Harwood, D.M., Barrett, P.J., Edwards, A.R., Rieck, H.J., and Webb, P.-N., 1989, Biostratigraphy and chronology, *in* Barrett, P.J., ed., Antarctic Cenozoic history from the CIROS-1 drillhole, McMurdo Sound, DSIR Bulletin 245, p. 231-239.

Hayes, D.E., and Davey, F.J., 1975, A geophysical study of the Ross Sea, Antarctica, *in* Hayes, D.E., and Frakes, L.A., eds., Initial Reports of the Deep Sea Drilling Project 28: Washington, DC, US Government Printing Office, p. 887-907, doi: 10.2973/dsdp.proc.28.134.1975

Hayes, D.E. and Frakes, L.A., 1975, General synthesis, Deep-Sea Drilling Project Leg 28, *in* Hayes, D.E., and Frakes, L.A., eds., Initial Reports of the Deep Sea Drilling Project 28: Washington, DC, US Government Printing Office, p. 919-942, doi: 10.2973/dsdp.proc.28.136.1975.

Hayes, D.E., and The Shipboard Scientific Party, 1975a, Sites 270, 271, 272, Deep-Sea Drilling Project Leg 28, *in* Hayes, D.E., and Frakes, L.A., eds., Initial Reports of the Deep Sea Drilling Project 28: Washington, DC, US Government Printing Office, p. 211-334, doi: 10.2973/dsdp.proc.28.106.1975.

Hayes, D.E., and The Shipboard Scientific Party, 1975b, Site 273, Deep-Sea Drilling Project Leg 28, *in* Hayes, D.E., and Frakes, L.A., eds., Initial Reports of the Deep Sea Drilling Project

28: Washington, DC, US Government Printing Office, p. 335-367, doi: 10.2973/dsdp.proc.28.109.1975.

Henrys, S.A., Bucker, C.J., Bartek, L.R., Bannister, S., Niessen, F., and Wonik, T., 2000, Correlation of seismic reflectors with CRP-2/2A, Victoria Land Basin, Antarctica: Terra Antarctica, v. 7, no. 3, p. 221-230.

Henrys, S.A., Bucker, C.J., Niessen, F., and Bartek, L.R., 2001, Correlation of seismic reflectors with the CRP-3 drillhole, Victoria Land Basin, Antarctica: Terra Antarctica, v. 8, no. 3, p. 127-136.

Henrys, S., Wilson, T., Whittaker, J.M., Fielding, C., Hall, J., and Naish, T., 2007, Tectonic history of mid-Miocene to present southern Victoria Land Basin, inferred from seismic stratigraphy in McMurdo Sound, Antarctica: U.S. Geological Survey and The National Academies Open-file Report 2007-1047, Short Research Paper 049, doi: 10.3133/of2007-1047.srp049.

Hinz, K., and Block, M., 1984, Results of geophysical investigations in the Weddell Sea and in the Ross Sea, Antarctica, *in* Proceedings, World Petroleum Congress, v. 11, no. 2, p. 79-91.

Hole, M.J., and LeMasurier, W.E., 1994, Tectonic controls on the geochemical composition of Cenozoic, mafic alkaline volcanic rocks from West Antarctica: Contrib Mineral Petrol, v. 117, p. 187-202.

Horgan, H., Naish, T., Bannister, S., Balfour, N., and Wilson, G., 2005, Seismic stratigraphy of the Plio-Pleistocene Ross Island flexural moat-fill: a prognosis for ANDRILL Program drilling beneath McMurdo-Ross Ice Shelf: Global and Planetary Change, v. 45, no. 1-3, p. 83-97.

Huerta, A.D., and Harry, D.L., 2007, The transition from diffuse to focused extension: Modeled evolution of the West Antarctic Rift system: Earth and Planetary Science Letters, v. 255, no. 1-2, p. 133-147.

Jha, S., Witt, D.R., and Harry, D.L., 2013, Flexural rigidity around Ross Island, Antarctica based on geodynamic modeling and seismic stratigraphy, Abstract T13A-2518 presented at 2013 Fall Meeting, American Geophysical Union, San Francisco, Calif., 9-13 Dec.

Jha, S., Harry, D.L., and Wenman, C.P., 2015, Seismic stratigraphic mapping and evolution of the Ross Island flexural basin in western Antarctica over the past ~5 Ma, Abstract 301 presented at 2015 International Symposium on Antarctic Earth Science (ISAES), The Scientific Committee on Antarctic Research (SCAR), Goa, India, 13-17 Jul.

Karner, G.D., Studinger, M., and Bell, R.E., 2005, Gravity anomalies of sedimentary basins and their mechanical implications: Application to the Ross Sea basins, West Antarctica: Earth and Planetary Science Letters, v. 235, no. 3-4, p. 577-596.

Krissek, L., Browne, G., Carter, L., Cowan, E., Dunbar, G., McKay, R., Naish, T., Powell, R., Reed, J., and Wilch, T., ANDRILL-MIS Science Team, 2007, Sedimentology and Stratigraphy of the AND-1B Core, ANDRILL McMurdo Ice Shelf Project, Antarctica: ANDRILL Research and Publications, Paper 22, p. 185-222.

Kyle, P.R., 1990, McMurdo Volcanic Group – Western Ross Embayment: Introduction, *in* LeMasurier, W.E., and Thomson, J.W., eds., Volcanoes of the Antarctic Plate and Southern Oceans, Antarctic Research Series, v. 48, American Geophysical Union, Washington, D.C., p. 19-25.

Kyle, P.R., and Cole, J.W., 1974, Structural Control of Volcanism in the McMurdo Volcanic Group, Antarctica: Bulletin of Volcanology, v. 38, no. 1, p. 16-35.

Lawver, L.A., and Gahagan, L.M., 1994, Constraints on Timing of Extension in the Ross Sea Region: Terra Antarctica, v. 1, no. 3, p. 545-552.

LeMasurier, W.E., and Rex, D.C., 1991, The Marie Byrd Land volcanic province and its relation to Cainozoic West Antarctic rift system, *in* Tingey, R.J., ed., The geology of Antarctica: New York, Oxford University Press, p. 249-284.

LeMasurier, W.E., and Landis, C.A., 1996, Mantle-plume activity recorded by low-relief erosion surfaces in West Antarctica and New Zealand: GSA Bulletin, v. 108, no. 11, p. 1450-1466.

Luyendyk, B.P., 1995, Hypothesis for Cretaceous rifting of East Gondwana caused by subducted slab capture: Geology, v. 23, no. 4, p. 373-376.

Luyendyk, B.P., Cisowski, S., Smith, C.H., Richard, S.M., and Kimbrough, D.L., 1996, Paleomagnetic study of northern Ford Ranges, western Marie Byrd Land, West Antarctica: A middle Cretaceous pole, and motion between West and East Antarctica?: Tectonics, v. 15, no. 1, p. 122-14, doi: 10.1029/95TC02524.

Luyendyk, B.P., Sorlien, C.C., Wilson, D.S., Bartek, L.R., and Siddoway, C.S., 2001, Structural and tectonic evolution of the Ross Sea rift in the Cape Colbeck region, Eastern Ross Sea, Antarctica: Tectonics, v. 20, no. 6, p. 933-958.

Luyendyk, B.P., Wilson, D.S., and Siddoway, C.S., 2003, Eastern margin of the Ross Sea Rift in western Marie Byrd Land, Antarctica: Crustal structure and tectonic development: Geochemistry Geophysics Geosystems, v. 4, no. 10, 1090, doi: 10.1029/2002GC000462.

Mukasa, S.B., and Dalziel, I.W.D., 2000, Marie Byrd Land, West Antarctica: Evolution of Gondwana's Pacific margin constrained by zircon U-Pb geochronology and feldspar common-Pb isotopic compositions: GSA Bulletin, v. 112, no. 4, p. 611-627.

Müller, R.D., Cande, S.C., Stock, J.M., and Keller, W.R., 2005, Crustal structure and rift flank uplift of the Adare Trough, Antarctica: Geochemistry Geophysics Geosystems, v. 6, no. 11, Q11010, doi: 10.1029/2005GC001027.

Müller, R.D., Gohl, K., Cande, S.C., Goncharov, A., and Golynsky, A.V., 2007, Eocene to Miocene geometry of the West Antarctic Rift System: Australian Journal of Earth Sciences, v. 54, p. 1033-1045.

Naish, T., Powell, R., Levy, R., and ANDRILL-MIS Science Team, 2007a, Background to the ANDRILL McMurdo Ice Shelf Project (Antarctica) and Initial Science Volume: Terra Antarctica, v. 14, no. 3, p. 121-130.

Naish, T., Powell, R., Levy, R., Henrys, S., Krissek, L., Niessen, F., Pompilio, M., Scherer, R., Wilson, G., and ANDRILL-MIS Science Team, 2007b, Synthesis of the Initial Scientific Results of the MIS Project (AND-1B Core), Victoria Land Basin, Antarctica: Terra Antarctica, v. 14, no. 3, p. 317-327.

Niessen, F., Magens, D. and Gebhardt, A.C., 2007, Physical properties measured on the ANDRILL AND-1B drill core, doi: 10.1594/PANGAEA.676905, *supplement to* Niessen, F., Magens, D. and Gebhardt, A.C., 2007, Physical properties of the ANDRILL AND-1B core, ANDRILL McMurdo Ice Shelf Project, Antarctica: Terra Antarctica, v. 14, no. 3, p. 155-166.

Niessen, F., Gebhardt, A.C., Kuhn, G., Magens, D., and Monien, D., 2014, Physical properties of ANDRILL AND-1B sediment core, doi: 10.1594/PANGAEA.834617, *supplement to* Niessen, F., Gebhardt, A.C., Kuhn, G., Magens, D., and Monien, D., 2013, Porosity and density of the AND-1B sediment core, McMurdo Sound Region, Antarctica: Field

consolidation enhanced by grounded ice: Geosphere, v. 9, no. 3, p. 489-509, doi: 10.1130/GES00704.1.

Pekar, S.F., Speece, M.A., Wilson, G.S., Sunwall, D.S., and Tinto, K.J., 2013, The Offshore New Harbour Project: deciphering the Middle Miocene through Late Eocene seismic stratigraphy of Offshore New Harbour, western Ross Sea, Antarctica, *in* Hambrey, M.J., Barker, P.F., Barrett, P.J., Bowman, V., Davies, B., Smallie, J.L., and Tranter, M., eds., Antarctic Palaeoenvironments and Earth-Surface Processes, 2013, Geological Society, London, Special Publications, v. 381, p. 199-213, doi: 10.1144/SP381.2.

Pollard, D., and DeConto, R.M., 2009, Modelling West Antarctic ice sheet growth and collapse through the past five million years: Nature, v. 458, p. 329-332, doi: 10.1038/nature07809.

Press, F., 1966, Section 9: Seismic velocities: Geological Society of America Memoirs, v. 97, p. 195-218.

Rilling, S.E., Mukasa, S.B., Wilson, T.J., and Lawver, L.A., 2007, ^{40}Ar-^{39}Ar Age constraints on volcanism and tectonism in the Terror Rift of the Ross Sea, Antarctica: U.S. Geological Survey and The National Academies Open-file report 2007-1047, Short Research Paper 092, doi: 10.3133/of2007-1047.srp092.

Ross, J.I., McIntosh, W.C., and Dunbar, N.W., 2012, Development of a precise and accurate age-depth model based on ^{40}Ar/^{39}Ar dating of volcanic material in the ANDRILL (1B) drill core, Southern McMurdo Sound, Antarctica: Global and Planetary Change, v. 96-97, p. 118-130.

Sieminski, A., Debayle, E., Lévêque, J.-J., 2003, Seismic evidence for deep low-velocity anomalies in the transition zone beneath West Antarctica: Earth and Planetary Science Letters, v. 216, no. 4, p. 645-661.

Speece, M.A., Levy, R.H., Harwood, D.M., Pekar, S.F., and Powell, R.D., 2009, New Seismic Methods to Support Sea-Ice Platform Drilling: Scientific Drilling, no. 7, p. 40-43, doi: 10.2204/iodp.sd.7.06.2009.

Stern, T.A., Davey, F.J., and DeLisle, G., 1991, Lithospheric flexure induced by the load of Ross Archipelago, southern Victoria Land, Antarctica, *in* Thomson, M.R.A., Crame, J.A., and Thomson, J.W., eds., Geological Evolution of Antarctica: Cambridge University Press, New York, pp. 323-328.

Storey, B.C., Alabaster, T., Hole, M.J., Pankhurst, R.J., Wever, H.E., 1992, Role of subduction-plate boundary forces during the initial stages of Gondwana break-up: evidence from the proto-Pacific margin of Antarctica, *in* Alabaster, B.C., and Pankhurst, R.J., eds., Magmatism and the Causes of Continental Break-up, 1992, Geological Society Special Publication, no. 68, p. 149-163.

Sunwall, D.A., Speece, M.A., and Pekar, S.F., 2012, Advances in on-sea-ice seismic reflection methods using an air gun: McMurdo Sound, Antarctica: Geophysics, v. 77, no. 1, p. S19-S30, doi: 10.1190/GEO2011-0127.1.

Torsvik, T.H., Gaina, C., and Redfield, T.F., 2007, Antarctica and Global Paleogeography: From Rodinia, Through Gondwanaland and Pangea, to the Birth of the Southern Ocean and the Opening of Gateways, *in* Cooper, A.K., Barrett, P.J., Stagg, H., Storey, B., Stump, E., Wise, W., and the 10th ISAES team, eds., Antarctica: A Keystone in a Changin World: Proceedings of the 10th International Symposium on Antarctic Earth Sciences, 2008, Washington, D.C., The National Academies Press, doi: 10.3133/of2007-1047.kp11.

Weaver, S.D., Storey, B.C., Pankhurst, R.J., Mukasa, S.B., DiVenere, V.J., and Bradshaw, J.D., 1994, Antarctica-New Zealand rifting and Marie Byrd Land lithospheric magmatism linked to ridge subduction and mantle plume activity: Geology, v. 22, no. 9, p. 811-814.

Webb, P.-N., 1983, Climatic, palaeo-oceanographic and tectonic interpretation of Palaeogene-Neogene biostratigraphy from MSSTS-1 drillhole, McMurdo Sound, Antarctica, *in* Oliver, R.L., James, P.R., and Jago, J.B., eds., Antarctic earth sciences: Canberra, Australian Academy of Science, p. 560.

White, P., 1998, Density, Porosity, Gamma ray of station CIROS-1, doi: 10.1594/PANGAEA.54716, *supplement to* White, P., 1989, Downhole logging, *in* Barrett, P.J., ed., Antarctic Cenozoic history from the CIROS-1 drillhole, McMurdo Sound: DSIR Bulletin, DSIR Publishing, Wellington, New Zealand, v. 245, p. 7-14.

Wilson, G.S., Roberts, A.P., Verosub, K.L., Florindo, F., and Sagnotti, L., 1998, Magnetobiostratigraphic chronology of the Eocene-Oligocene transition in the CIROS-1 core, Victoria Land margin, Antarctica: Implications for Antarctic glacial history: GSA Bulletin, v. 110, no. 1, p. 35-47.

Wilson, G.S., Levy, R.H., Browne, G., Cody, R., Dunbar, N., Florindo, F., Henrys, S., Graham, I., McIntosh, W., McKay R., Naish, T.R., Ohneiser, C., Powell, R.D., Ross, J., Sagnotti, L., Scherer, R., Sjunneskog, C., Strong, C.P., Taviani, M., Winter, D., and ANDRILL-MIS Science Team, 2007, Preliminary Integrated Chronostratigraphy of the AND-1B Core, ANDRILL McMurdo Ice Shelf Project, Antarctica: ANDRILL Research and Publications, Paper 46, p. 297-316.